The riddle of eastern tropical Pacific ocean oxygen levels : the role of the supply by intermediate depth waters.

Olaf Duteil (oduteil@geomar.de)(1), Ivy Frenger(1), Julia Getzlaff(1)
(1) GEOMAR, Kiel, Germany

Abstract

~~It is well known that Intermediate Water Masses (IWM) are sinking in high latitudes and ventilate the lower thermocline (500 – 1500 m depth). We here highlight how the IWM oxygen content and the IWM pathway along the Equatorial Intermediate Current System (EICS) towards the eastern tropical Pacific ocean are essential for the supply of oxygen to the lower thermocline and the Oxygen Minimum Zones (OMZs). To this end, we assess here a heterogeneous subset of ocean models characterized by a horizontal resolution ranging from 0.1° to 2.8°. Subtropical oxygen levels in the lower thermocline, i.e., IWM are statistically correlated with tropical oxygen levels and OMZs. Sensitivity simulations suggest that the oxygen biases of the subtropical IWM oxygen levels contribute to oxygen biases of the tropical thermocline : an increase of the IWM oxygen by 60 mmol.m^{-3} results in a 10 mmol.m^{-3} increase in the tropical ocean in a timescale of 50 years. In the equatorial regions, the IWM recirculates into the Equatorial Intermediate Current System (EICS). By comparing tracer and particle release simulations, we show that a developed EICS increases eastern tropical ventilation by 30 %. Typical climate models lack in representing crucial aspects of this supply: biases in IWM properties are prominent across climate models and the EICS is basically absent in models with typical resolutions of ~1°. We emphasize that these biases need to be reduced in global climate models to allow reliable projections of OMZs in a changing climate.~~

Observed Oxygen Minimum Zones (OMZs) in the tropical Pacific ocean are located above intermediate depth waters (IDW). Typical climate models do not represent correctly IDW properties and are characterized by a too deep reaching OMZ. We test here the role of the IDW on the misrepresentation of oxygen levels in a heterogeneous subset of ocean models characterized by a horizontal resolution ranging from 0.1° to 2.8°. First, we show that forcing the extra tropical boundaries (30°S/N) to observed oxygen values results in a significant increase of oxygen levels in the intermediate eastern tropical region. Second, the equatorial intermediate current system (EICS) is a key feature connecting the western and eastern part of the basin. Typical climate models lack in representing crucial aspects of this supply at intermediate depth, as the EICS is basically absent in models characterized by a resolution lower than 0.25°. These two aspects add up to a “cascade of biases”, that hampers the correct representation of oxygen levels at intermediate depth in the eastern tropical Pacific Ocean and potentially future OMZs projections.

1. Introduction

Oxygen levels in the ocean are characterized by high values in the high latitudes and the subtropical gyres, while concentrations decrease to close to zero in the tropical oceans in the Oxygen Minimum Zones (OMZs). While OMZs are natural features, climate change is potentially responsible for their expansion (Breitburg et al., 2018), leading to a reshaping of the ecosystems and a potential loss of biodiversity.

Modelling oxygen levels is particularly challenging because of the complexity of the interactions between biological respiration and physical transport (e.g Deutsch et al., 2014, Ito et al., 2013; Duteil et al., 2014a,b, 2018, Oschlies et al., 2017). Climate models tend to overestimate the volume of the OMZs (Cabre et al., 2015) and do not agree on the intensity and even sign of oxygen future evolution (Oschlies et al., 2017). In order to perform robust projections there is a need to better understand the processes at play that are responsible for the supply of oxygen to the OMZ. We focus here on the Pacific ocean, where large OMZs are located in a depth range from 100 to 900 m (Karstensen et al., 2008; Paulmier and Ruiz-Pino. 2009). Previous modelling studies have shown that the tropical OMZ extension is at least partly controlled by connections with the subtropical ocean (Duteil et al., 2014). In addition, the role of the equatorial undercurrent (Shigemitsu et al., 2017; Duteil et al., 2018; Busecke et al., 2019), of the secondary Southern Subsurface Countercurrent (Montes et al, 2014), of the interior eddy activity (Frenger et al., 2018), have been previously highlighted. These studies focus on the mechanisms at play in the upper oxygen levels (upper 500 m meter). The oxygen content below the core of the OMZ however plays a significant role in setting the upper oxygen levels by diffusive (Duteil and Oschlies, 2009) or vertical advective (Duteil, 2019) processes. Here, we focus specifically on the mechanisms supplying oxygen toward the eastern tropical pacific ocean at intermediate depth (500 – 1500 m), below the OMZ core.

The water masses occupying this intermediate depth layer (500 – 1500 m) (Emery, 2003) subduct at high latitudes (Karstensen et al., 2008). Oxygen solubility increases with lower temperatures, thus waters formed in the Southern Ocean and in the North Pacific are characterized by high oxygen values. In particular, the Antarctic Intermediate Water (AAIW) (Molinelli, 1981) ventilates large areas of the lower thermocline of the Pacific Ocean (Sloyan and Rintoul., 2001) and is characterized by oxygen values larger than 300 $mmol.m^{-3}$ at subduction time (Russel and Dickson, 2003). The oxygenated core of the AAIW in the tropical Pacific is located at about 500-1200 m depth at 40°S (Russell and Dickson, 2003) and with this at a depth directly below the depth of the OMZs in the eastern Pacific; the Pacific AAIW mixes down to 2000 m depth with the oxygen poor Pacific Deep Water (PDW) as determined by the OMP (Optimum Multiparameter) analysis (Pardo et al., 2012; Carrasco et al., 2017). The oxygen rich (> 200 $mmol.m^{-3}$ at 40°S) AAIW spreads from

its formation side in the Southern Ocean to the subtropical regions. The northern part of the Pacific basin is characterized by the North Pacific Intermediate Water (NPIW) (Talley, 1993) confined to the northern Pacific conversely to the AAIW, which spreads far northward as its signature reaches 15°N (Qu and Lindstrom., 2004). AAIW, NPIW and the upper part of the PDW are oxygenated water masses occupying the lower thermocline between 500 and 1500 m depth. In this study we do not specifically focus on the individual water masses, but rather on the water occupying the intermediate water depth (500 – 1500 m) (Emery, 2003) of the subtropical and tropical ocean. We will refer to the waters in this depth range as intermediate depth waters (IDW).

In the subtropics, the IDW (particularly the AAIW) circulates into the intermediate flow of the South Equatorial Current and the New Guinea Coastal Undercurrent (Qu and Lindstrom, 2004) where it retroflects in the zonal equatorial flows of the Southern Intermediate Countercurrent (SICC) and Northern Equatorial Intermediate Current (NEIC) within about ±2° off the equator (Zenk et al., 2005; Kawabe et al., 2010) (Fig 1). These currents are part of the Equatorial Intermediate Current System (EICS) constituted by a complex system of narrow jets extending below 500 m in the lower thermocline (Firing, 1987; Ascani et al., 2010; Marin et al. 2010; Cravatte et al., 2012, 2017; Menesguen et al., 2019). While the existence of this complex jet system has been shown to exist in particular using argo floats displacements (Cravatte et al., 2017) the spatial structure and variability of the jets are still largely unknown. In addition, there is little knowledge about their role in transporting properties such as oxygen.

The simulation of the supply of oxygen to the eastern tropical Pacific below the OMZ core is a difficult task as it depends on the realistic simulation of the IDW properties (in particular the oxygen content) and the IDW pathway (through the EICS). It is known that current climate models, in particular CMIP5 (Coupled Model Intercomparison Project phase 5) models, have deficiencies in correctly representing the IDW, and in particular the AAIW. They generally display too shallow and thin IDW, with a limited equatorward extension compared to observations (Sloyan and Kamenkovich, 2007; Sallee et al., 2013; Meijers, 2014; Cabre et al., 2015; Zhu et al., 2018 for the south Atlantic ocean). Discrepancies in the simulated properties of IDW compared to observations are due to a combination of a range of errors in the climate models, including in the simulation of wind and buoyancy forcing, an inadequate representation of subgrid-scale mixing processes in the Southern Ocean, and midlatitude diapycnal mixing parameterizations (Sloyan and Kamakovich, 2007; Zhu et al., 2018). In addition, the EICS is mostly lacking in coarse resolution models (Dietze and Loeptien, 2013; Getzlaff and Dietze, 2013). Higher resolution (0.25°, 1/12°) configurations partly resolve the EICS but with smaller current speeds than observed (Eden and Dengler, 2008; Ascani et al., 2015). The mechanisms forcing the EICS are complex and still under debate (see the review by Menesguen et al., 2019).

3

In this study we focus on the impact of IDW (and of the deficiencies in the representation of their properties and transport) on the oxygen content in the eastern tropical Pacific in a set of model simulations. Section 2 gives an overview of all models that we used as well as of the sensitivity simulations. Next, we assess to which extent the IDW modulate (or drive) the oxygen levels in the eastern tropical (20°S – 20°N; 160°W-coast) Pacific ocean in this set of models. The role of the IDW depends i) on the oxygen content of the IDW in the lower thermocline of the subtropical regions (section 3) and ii) on the zonal recirculation of the oxygen by the EICS toward the eastern part of the basin (section 4). We conclude in section 5.

2. Analyzed models and experiments

2.1 Mean state

We analyze the mean state of the oxygen fields, OMZ, EICS of the following model experiments (see Table 1), which previously have been used in recent studies focusing on the understanding of the tropical oxygen levels mean state or variability :

- the NEMO (Nucleus for European Modelling of the Ocean) model (Madec et al., 2017) with a resolution of 2°, refined meridionally to 0.5° in the equatorial region (NEMO2 configuration). The circulation model is coupled to a simple NPZD (Nutrient Phytoplankton Zooplankton Detritus) biogeochemical model that comprises 6 compartments (e.g used in Duteil et al., 2018; Duteil, 2019). The simulation has been forced by climatological forcings based on the Coordinated Reference Experiments (CORE) v2 reanalysis (Normal Year Forcing) (Large and Yeager, 2009) and integrated for 1000 years.
- the UVIC (University of Victoria) model (e.g used in Getzlaff et al., 2016; Oschlies et al., 2017), an earth System Model (ESM) that has a horizontal resolution of 1.8° latitude x 3.6° longitude. The experiment has been integrated for 10000 years. The biogeochemical model is a NPZD-type model of intermediate complexity that describes the full carbon cycle (see Keller et al., 2012 for a detailed description). This model is forced by monthly climatological NCAR/NCEP wind stress fields.
- the GFDL (Geophysical Fluid Dynamics Laboratory) CM2-0 suite (Delworth et al., 2012; Griffies et al., 2015, Dufour et al, 2015): the suite is based on the GFDL global climate model and includes a fully coupled atmosphere with a resolution of approximately 50 km. It consists of three configurations that differ in their ocean horizontal resolutions: GFDL1 with a nominal 1° resolution, GFDL025 with a nominal 0.25° and GFDL01 with a nominal 0.1° resolution (e.g used in Frenger et al., 2018 and Busecke et al., 2019 for studies on ocean oxygen). At simulation year 48, the simplified ocean biogeochemistry model miniBLING is coupled to the models, with three prognostic tracers, phosphate, dissolved inorganic carbon and oxygen (Galbraith et al., 2015). Due to the high resolution of GFDL01, the integration time is limited. We here analyze simulation years 186 to 190.

4

All the models (NEMO2, UVIC, GFDL suite) are forced using preindustrial atmospheric pCO2 concentrations.

Differences in model resolution but also in atmosphere forcings or spinup duration strongly impact oxygen distribution (see Annex A). However, the heterogeneity of the configurations that we analyze permits to determine whether the simulated oxygen distributions display systematic biases / similar patterns.

The mean states of the oxygen distributions are discussed below in section 3.1 "IDW Oxygen levels in models".

2.2 Sensitivity simulations

In order to disentangle the different processes at play we perform two different sets of sensitivity simulations using the eNEMO model engine. NEMO allows to test effects of increasing the ocean resolution and to integrate the model over a relatively long time span. All sensitivity experiments are integrated for 60 years (1948 to 2007) using the CORE (Coordinated Ocean-Ice Reference Experiments) v2 interannual (Large and Yeager, 2009) forcings. This time scale permits the recirculation from the interior subtropical regions to the tropical area (as suggested in the model study by SenGupta and England, 2007).

2.2.1 Forcing of oxygen to observed values in the subtropical regions

In the first set of experiments the focus is on the role of the lower thermocline oxygen content for the ventilation of the eastern equatorial Pacific. We use NEMO2, the oceanic component of the IPSL-CM5A (Mignot et al., 2013), that is part of CMIP5. NEMO2 shows mid-latitudes oxygen biases consistent with CMIP5 models. We compare three experiments :

- NEMO2-REF: the experiment is integrated from 1948 to 2007 starting from the spinup state described in 2.1.
- NEMO2-30S30N: the oxygen boundaries are forced to observed oxygen concentrations (WOA) at the boundaries 30°N and 30°S: the mid-latitude oxygen levels in the IDW are therefore correctly represented.
- NEMO2-30S30N1500M: same as NEMOO2-30S30N; in addition oxygen is forced to observed concentrations at the depth interface of 1500m, mimicking a correct oxygen state of the deeper water masses (lower part of the AAIW, upper part of the PDW)

With the above three experiments we focus on the transport of IDW oxygen levels to the tropical ocean and the OMZs. The respiration rate (oxygen consumption) is identical in NEMO2-REF, NEMO2-30S30N and NEMO2-30S30N1500M in order to avoid compensating effects between

supply and respiration that depend on biogeochemical parameterizations (e.g Duteil et al., 2012). We aim to avoid such compensating effects to ease interpretation and be able to focus on the role of the physical transport. The sensitivity of tropical IDW oxygen to subtropical and deep oxygen levels is discussed in section 3.2

2.2.2 Conservative Tracer Release in oxygenated waters

In a second set of experiments, we assessed the effect of a resolution increase on the transport of a conservative tracer. To do this, we used a 0.5° (NEMO05) and a higher resolution 0.1° (NEMO01) configuration of the NEMO model engine (Table 1) to examine the transport of oxygenated IDW from the subtropical regions into the oxygen deficient tropics. NEMO01 is a configuration based on NEMO05 and where a 0.1° two-ways nest has been embedded in the whole Pacific Ocean, from 49°S to 31°N (Czeschel et al, 2011). In these experiments, we initialized the regions with climatological (WOA) oxygen levels greater than 150 $mmol.m^{-3}$ with a value of 1 (and 0 when oxygen was lower than 150 $mmol.m^{-3}$). In the model simulations, the tracer is subject to the same physical processes as other physical and biogeochemical tracers, i.e. advection and diffusion but it does not have any sources and sinks. The experiments have been integrated for 60 years (1948 – 2007) using realistic atmospheric forcing (COREv2). NEMO05 and NEMO01 display a similar upper ocean circulation (Fig 5) but NEMO05 does not simulate a developed EICS in contrast to NEMO01.

In order to complement the tracer experiment we performed Lagrangian particle releases. Lagrangian particles allow to trace the pathways of water parcels due to the resolved currents, and to track the origin and fate of water parcels. They are not affected by subgrid scale diffusive and advective processes. The particles are advected offline with 5 days mean of the NEMO05 and NEMO01 currents. The NEMO01 circulation fields have been interpolated to the NEMO05 grid in order to allow a comparison of the large scale advective patterns between NEMO01 and NEMO05. We used the ARIANE tool (Blanke and Raynaud, 1997). A first particle release has been performed in the eastern tropical OMZ at 100°W in the tropical region between 5°S - 5°N, a second release has been performed in the western part of the basin at 160°E. The particles have been released in the lower thermocline at 1000 m and integrated backward in time from 2007 to 1948 in order to determine their pathways and their location of origin. We released 120 particles every 5 days during the last year of the experiment, for a total of 8760 particles. The transport by the EICS is discussed in section 4.2 (tracers levels and Lagrangian pathways).

3. Intermediate water properties and oxygen content

3.1. IDW Oxygen levels in models

6

The IDW subducted in mid/high latitudes are highly oxygenated waters. As part of the deficient representation of IDW, the subducted “oxygen tongue” (oxygen values up to 240 mmol.m^{-3}) is not reproduced in most of the models part of CMIP5 (Fig 8 from Cabre et al., 2015, Fig 4 from Takano et al., 2018) and in the models analyzed here (Fig 2a), with an underestimation of about 20-60 mmol.m^{-3} (NEMO2, GFDL1, GFDL025, GFDL01). UVIC, a coarse resolution model, shows oxygenated waters in the lower thermocline at mid latitudes (30°S-50°S); the oxygenation however likely arises due to a too large vertical diffusion from the mixed layer rather than by an accurate representation of the water masses.

GFDL01, even though still biased low, presents larger oxygen values than the coarser resolution models GFDL1, GFDL025 and NEMO2. A possible explanation is a better representation of the water masses and in particular the AAIW in eddy-resolving models (Lackhar et al., 2009).

The IDW oxygen maximum is apparent at 30°S throughout the lower thermocline (600 – 1000 m) in observations (Fig 2b), consistent with the circulation of IDW with the gyre from the mid/high latitude formation regions towards the northwest in subtropical latitudes, and followed by a deflection of the waters in the tropics towards the eastern basin. This oxygen peak is missing in all the models analyzed here.

Consistent with the low oxygen bias of models at subtropical latitudes (Fig 2b), models also feature a bias in the tropical ocean (20°S-20°N) by 20 – 50 mmol.m^{-3} (Fig 2a, Fig 2c) at intermediate depths in the eastern part of the basin (similarly to CMIP5 models, as shown by Cabre et al., 2015). The basin zonal average of the mean oxygen level in the lower thermocline layer (500 - 1500m) at 30°S and in the eastern part of the basin (average 20°S – 20°N, 160°W-coast; 500-1500 m) are positively correlated (Pearson correlation coefficient R=0.73) (Fig 2d, Annex A), suggesting that the oxygen levels in the tropical pacific ocean are partly controlled by extra-tropical oxygen concentrations at intermediate depths and the associated water masses.

The models presenting the poorest oxygenated water at 30°S display the largest volume of OMZs (GFDL025 and GFDL1), though the negative correlation (Pearson correlation coefficient R=-0.52) is less pronounced between the volume of the OMZs and the mean oxygen levels in the layer 500 - 1500 m at 30°S (Fig 2e). Reasons for this weaker correlation are due to the OMZs being a result of several processes next to oxygen supply by IDW, e.g, vertical mixing with other water masses (Duteil et al., 2011), isopycnal mixing in the upper thermocline (Gnanadesikan et al., 2013; Bahl et al., 2019), supply by the upper thermocline circulation (Shigemitsu et al., 2017; Busecke et al., 2019). A correlation, even weak, suggests a major role of the IDW in regulating the OMZ volume.

7

In order to better understand the role of IDW entering the subtropical domain from higher latitudes for the oxygen levels in the eastern tropical Pacific Ocean, we perform sensitivity experiments (see 2.2.1) in the following.

3.2 Sensitivity of tropical IDW oxygen to subtropical and deep oxygen levels

3.2.1 Oxygen levels in the lower thermocline

The difference of the experiments NEMO2-30S30N – NEMO2-REF (average 1997-2007) (Fig 3c,d) allows to quantify the effect of model biases of IDW at mid latitudes (30°N/30°S) on tropical oxygen levels. As we restore oxygen to observed levels at 30°S/°N (see 2.2.1), the difference between both experiments shows a large anomaly in oxygen levels at 30°S (more than 50 mmol.m^{-3}) at lower thermocline level (500 – 1500 m) corresponding to the missing deep oxygen maximum, located in the IDW. The northern negative anomaly results from a deficient representation of the north Pacific OMZ, i.e., modeled oxygen is too high for NPIW. The northern low and southern high anomalies spread towards the tropics at intermediate depth. A fraction of the positive oxygen anomaly recirculates at upper thermocline level due to a combination of upwelling and zonal advection by the tropical current system (for instance the EUC at thermocline level is a major supplier of oxygen as shown in observations by Stramma et al., 2010 and in ocean models by Duteil et al., 2014, Busecke et al., 2019).

The difference NEMO2-30S30N1500M – NEMO2-30S30N (Fig 3e,f) shows a deep positive anomaly in oxygen, as oxygen levels are lower than in observations by 30-40 mmol.m^{-3} in the eastern tropical regions. This anomaly is partially transported into the IDW (500 - 1500 m). It shows that a proper representation of the deep oxygen levels (> 1500 m) is important for a realistic representation of the lower thermocline and OMZs. Causes of the oxygen bias of the deeper water masses are beyond the scope of this study but may be associated with regional (tropical) issues, such as an improper parameterization of respiration (e.g a too deep remineralisation) (Kriest et al., 2010), or a misrepresentation of deeper water masses.

3.2.2 Oxygen budget and processes

To assess the processes that drive the oxygen content of the (sub)tropical lower thermocline, we analyzed the oxygen budget in NEMO2-REF and NEMO2-30S30N, NEMO30S30N1500M. The budget is computed as an average between 500 and 1500m and shown in Fig 3g and Fig.4.

The oxygen budget is :

$$\frac{\delta O_2}{\delta dt} = Adv_x + Adv_y + Adv_z + Diff_{Dia} + Diff_{Iso} + SMS$$

8

where Adv_x,Adv_y,Adv_z, are respectively the zonal, meridional and vertical advection terms, $Diff_{dia}$ and $Diff_{iso}$ are the diapycnal and isopycnal diffusion terms. SMS (Source Minus Sink) is the biogeochemical component (i.e below the euphotic zone this is only respiration)

In NEMO2-REF, the physical oxygen supply is balanced by the respiration. The oxygen supply in the model is divided into advection, i.e., oxygen transport associated with volume transport, and isopycnal diffusion, i.e., subgrid scale mixing processes that homogenize oxygen gradients (Fig 4a). Diapycnal diffusion is comparatively small and can be neglected.

The supply of oxygen from the high latitudes toward the tropical interior ocean is constituted by several processes acting concomitantly : isopycnal diffusion transfers oxygen from the oxygen-rich gyres to the poor oxygenated regions (see Fig 1). The lower branches of the subtropical gyres transport the oxygen from the eastern to the western part of the basin. Downwelling from the oxygen-rich mixed layer supplies the interior of the subtropical gyres. At the equator, the EICS transport westward oxygen-poor water originating in the eastern side of the basin (Fig 4a). The meridional advection term transports oxygen originating from the subtropics in the tropical regions, which is upwelled.

Forcing oxygen levels in NEMO2-30S30N at 30°S and 30°N creates an imbalance between respiration (which remains identical in NEMO2-REF and NEMO2-30S30N) and supply. This imbalance is most apparent in the tropics by an increase (south) or decrease (north) of isopycnal diffusion (Fig 3g, Fig 4b. Changes in the advective terms are found along the equator: as the vertical gradient of oxygen decreases (the intermediate ocean being more oxygenated), the vertical supply from the upper ocean decreases in the south (increases in the north) subtropical gyre and decreases at the equator (Fig 4b). The meridional oxygen gradient between the southern subtropical gyre and the equator strengthens, and so does the meridional transport from the subtropics to the equator, partly by the western boundary currents. The changes in zonal transport are comparatively small.

In the experiment NEMO2-30S30N1500, in complement to the isopycnal propagation of the subtropical anomaly, the deep (> 1500 m) oxygen anomaly is upwelled in the eastern equatorial (500 – 1500 m) part of the basin (see Fig 3g). The transport due to advective terms strongly increases, mostly due to an increase in vertical advection. This is consistent with the analysis by Duteil (2019) who showed that vertical advection is the dominant process to supply oxygen from the lower to the upper thermocline in the equatorial eastern Pacific Ocean in a similar NEMO2 configuration.

9

This simple set of experiments already shows that in climate models oxygen in the lower thermocline (500 – 1500 m) tropical ocean are partially controlled by properties of IDW that enter the tropics from higher latitudes. This presumably also applies to other (biogeochemical) tracers. IDW oxygen propagates equatorward mostly by small scale isopycnal processes and the western boundary currents. Further, upwelling in the tropics from deeper ocean layers (Pacific Deep Water, partially mixed with the lower IDW) play an important role. We will examine more closely in the following the representation and the role of the EICS in supplying oxygen toward the eastern Pacific Ocean.

4. Equatorial intermediate current system and oxygen transport

4.1 Structure of the currents in the upper 2000 m in observations and models

The current structure of the models analyzed in this study (see section 2.1, Table 1) is shown in Fig 5. In the mixed layer, the broad westward drifting South and North Equatorial Currents (SEC, NEC) characterize the equatorial side of subtropical gyres. In the thermocline, the eastward flowing equatorial undercurrent (EUC), flanked by the westward flowing south and north counter currents are present in all models. This upper current structure is well reproduced (i.e the spatial structure and intensity are consistent with observations) across the different models (see 2.1 “Model analyzed”) compared to observations. Previous studies already discussed the upper thermocline current structure in the GFDL models suite (Busecke et al., 2019), NEMO2 and NEMO05 (e.g Izumo, 2005, Lübbecke et al., 2008), UVIC (Loeptien and Dietze, 2013); the upper thermocline will not be further discussed in this study.

At intermediate depth, in the observations, a relatively strong (about 0.1 ms^{-1}) westward flowing Equatorial Intermediate Current (EIC) is present below the EUC at about 400-600 m depth (Marin et al., 2010). A complex structure of narrow and vertically alternating jets every 200 m, so-called Equatorial Deep Jets (EDJ), extends below the EIC till 2000 m (Firing, 1987; Cravatte et al., 2012). Laterally to the EIC, in the upper thermocline, the Low Latitude Subsurface Countercurrents (LLSC) are observed. They include the North and South Subsurface Counter Currents (NSCC and SSCC), located around 5°N/5°S, and a series of jets between 5°N/S and 15°N/S (in particular the Tsuchiya jets in the southern hemisphere, described by Rowe et al., 2000). Below the LLSCs, the Low Latitude Intermediate Currents (LLICs) include a series of westward and eastward zonal jets (500–1500-m depth range) alternating meridionally from 3°S to 3°N; the North and South Intermediate Countercurrents (NICC and SICC) flow eastward at 1.5°–2° on both flanks of the lower EIC. The North and South Equatorial Intermediate Currents (NEIC and SEIC) flow westward at about 3° (Firing, 1987). A detailed schematic view of the tropical intermediate circulation is shown in a recent review by Menesguen et al. (2019) and in Fig 1.

10

In coarse resolution models, the intermediate current system is not developed and sluggish (even missing in UVIC and GFDL1). NEMO2 and NEMO05 display a “primitive” EICS as the LLSCs are not represented. High resolution models (GFDL025, GFDL01, NEMO01) display a more realistic picture, even if the mean velocity is still weaker than in observations (smaller than 5 $cm.s^{-1}$), where it reaches more than 10 cm^{-1} at 1000 m (Ascani et al., 2010; Cravatte et al., 2017). An interesting feature is that the jets are broader and faster in NEMO01 than in GFDL01. Possible causes include a different wind forcing, mixing strength or topographic features as all these processes play a role in forcing the intermediate jets (see the review by Menesguen et al., 2019). The intermediate currents are less coherent vertically in NEMO01 than in GFDL01, due to their large temporal variability in NEMO01. A strong seasonal and interannual variability of the EICS has been observed that displays varying amplitudes and somewhat positions of the main currents/jets (Firing, 1998; Gouriou et al., 2006: Cravatte et al., 2017). A clear observational picture of the EICS variability is however not yet available. Outside the tropics (in particular south of 15°S), the interior velocity pattern is similar in coarse and high resolution models, suggesting a similar equatorward current transport at intermediate depth in the subtropics, in for instance NEMO05 and NEMO01.

4.2 Transport by the EICS

4.2.1 Tracer spreading towards the eastern tropical Pacific

We released a conservative tracer in the subtropical domain in well oxygenated waters (see 2.2.2) in a coarse (NEMO05) and a high resolution configuration (NEMO01). The tracer does not have sources or sinks and is advected and mixed as any other model tracer and allows to assess the transport pathway of tracer (such as oxygen) from oxygenated waters into the oxygen deficient eastern tropical Pacific.

The importance of the ventilation by the oxygen rich waters, and in particular the IDW, is illustrated by the tropical tracer concentration after 50 years (Fig 6a) of integration (mean 2002-2007). Concentrations decrease from the release location to the northern part of the basin, where the lowest values (below 0.1) are located in NEMO05 and NEMO01. The 0.1 isoline is however located close to the equator in NEMO05 while it is found around 7°N in NEMO01. This feature is associated with a pronounced tongue of high tracer concentration (> 0.2) between 5°N and 5°S in NEMO1. Such a tongue is absent in NEMO05. The enhanced tracer concentration in the equatorial region suggests a stronger zonal equatorial ventilation in NEMO01.

The preferential pathways of transport are highlighted by the determination of the transit time it takes for the tracer to spread from the oxygen rich regions to the tropical regions. We define a threshold called t10% when the tracer reaches a concentration of 0.1 (Fig 6b) (similar to the approach of SenGupta and England, 2007). t10% highlights a faster ventilation of the equatorial

11

regions in NEMO01 compared to NEMO05, as t10% displays a maximum value of 10 (western part) to 30 years (eastern part) between 5°N/5°S in NEMO01 compared to 30 years to more than 50 years in NEMO05. The southern “shadow zone” is well individualized in NEMO01 compared to NEMO05 as the oxygen levels are high in the equator in NEMO01, suggesting a strong transport by the EICS. The value of t10% increases linearly at intermediate depth at 100°W in NEMO05 from 20°S to the equator, suggesting a slow isopycnal propagation (consistent with the experiments performed using NEMO2 in part 3.2). Conversely, the tracer accumulation is faster in the equatorial regions than in the mid-latitudes in NEMO01, suggesting a large role of advective transport, which is faster than the transport by diffusive processes.

4.2.2 Equatorial lower thermocline water mass origin

Lagrangian particles (see 2.2.3) allow us to understand the origin of the waters in the lower thermocline. They also allow us to disentangle the transport of the resolved currents of the EICS (advection) from subgrid scale mixing processes, i.e. to assess the processes responsible for the equatorial ventilation. Two releases R1 and R2 have been performed in the eastern and western part of the basin in order to assess the equatorial circulation in NEMO05 and NEMO01. A depth horizon of 1000 m has been chosen as it is a depth where the equatorial intermediate current system is relatively well developed in high resolution models and basically absent in coarse models (see Fig 5). Our results are not sensitive to the choice of another depth horizon in the range of 500 - 1500 m

The release R1 i100°W, 5°N-5°S, 1000 m depth) is located in the larger intermediate eastern tropical pacific (IETP) ocean region (160°W – coast / 10°N-10°S / 200 – 2000 m). The particles originate close to the region of release (IETP) in 60 % of the cases in NEMO05 and 50 % of the cases in NEMO01, at a time scale of 50 years (Fig 7a and 8b). In NEMO05, after 50 years, the particles originating outside the IETP come either from the upper (0 – 200 m) ocean (5 %), deep (> 2000 m) ocean (1%), higher (> 10°) latitudes (23 %), western (west of 160°W) part of the basin (21 %) (Fig 8d). The largest difference between NEMO05 and NEMO01 is the much larger amount of particles originating from the deep ocean in NEMO01 (8 % in NEMO01), suggesting the presence of vertical recirculation cells at intermediate depths. Despite the stronger EICS in NEMO01, the amount of particles originating from the western part of the basin is nearly identical in NEMO01 and NEMO05 after 50 years of integration. The advection processes are however faster in NEMO01, in particular the zonal advection. The relative difference between NEMO05 and NEMO1 is particularly strong 15 years after the release (approximately corresponding to the t10% at 1000 m at the equator in NEMO01), as already 10 % of the particles originate outside the IETP, in regions where the oxygen levels are high, in NEMO01 while this fraction is close to 0 in NEMO05.

12

The second release R2 (160°E, 5°N-5°S, 1000 m depth) is located in the intermediate western tropical pacific (IWTP) ocean region (160°W – coast / 10°N-10°S / 200 – 2000 m) (Fig 7b). After 50 years, all the particles originate outside of the IWTP in NEMO01 (Fig 8c) (50 % originate in the eastern basin, 23 % in the deep ocean, 24 % outside the equatorial band, 3 % in the upper 200 m) (Fig 8e) while only 70 % of the particles originate outside the IWTP in NEMO05 (39 % in the eastern basin, 27 % outside the equatorial band, 2 % in the deep ocean and 2 % in the upper ocean).

The Lagrangian experiments show a generally stronger ventilation at intermediate depth in NEMO01 due to the EICS, which reinforces the connections between western / eastern part of the basin and the thermocline / deep ocean.

4.3 Model resolution and oxygen levels

~~Our analyses above permit to better understand the distribution of the oxygen levels at the equator in a suite of models characterized by an increasing resolution, such as the GFDL model suite. We decided to focus on the GFDL model suite here as they only differ by their resolution (same biogeochemical model). The striking difference between GFDL01 and GFDL025 / GFDL1 are the high oxygen levels in the eastern part of the ocean below 1000 m in GFDL01 compared to GFDL025/GFDL1 (Fig 2). The oxygen levels are also more homogeneous zonally in GFDL01, with a weaker east/west gradient, consistent with the tracer experiment that we performed in 4.2. The oxygen distribution fits with the mean kinetic energy of the intermediate currents below 1000 m (Fig 9a), especially in the eastern part of the basin (Fig 9b). Resolving the EICS results in a similar distribution as what Getzlaff and Dietze (2013) (GD13) achieved with a simple parameterization of the EICS (Fig 9a). To compensate for the "missing" EICS in coarse resolution models, they enhanced anisotropically the lateral diffusivity in the equatorial region.The oxygen levels from UVIC GD13 are shown in blue contours on top of the UVIC oxygen distribution in Fig 9. Implementing this approach tends to homogenize oxygen levels zonally, with an increase of the mean levels by 30-50 mmol.m^{-3} in the eastern basin and a decrease of oxygen concentrations in the western basin.~~

~~A possibly not intuitive feature is that the oxygen levels are relatively similar in GFDL025 and GFDL1, while the current system is relatively similar in GFDL025 and GFDL01 (see Fig 5 and Fig 9). An explanation lies in the relatively small net balance between large fluxes of respiration and oxygen supply (Duteil et al., 2014). If the supply is slightly higher compared to the consumption by respiration, it will lead to an increase of oxygen concentration. If it is slightly lower, the oxygen levels will decrease. A small difference in supply (e.g slightly weaker currents) may therefore lead~~

13

~~to a large difference in oxygen levels when integrated over decades. For this reason, the impact of the EICS is more visible below 1000 m as the respiration decreases following a power-law with depth (Martin et al., 1987) and is therefore easier to offset even by a moderate oxygen supply.~~

The experiments discussed in 4.2 were not coupled with biogeochemical cycles for computational cost reasons. In order to assess the robustness of our findings (EICS plays a large role in setting tropical oxygen levels), we next analyze equatorial oxygen in a set of climate models similar to CMIP models. To this end we use the GFDL model suite, characterized by a resolution increase (GFDL1, GFDL025 and GFDL01 - see Table 1).

The striking difference between GFDL01 and GFDL025 / GFDL1 are the high oxygen levels in the eastern part of the ocean below 1000 m in GFDL01 compared to GFDL025/GFDL1 (Fig 2). The oxygen levels show weaker zonal gradient in GFDL01, consistent with the tracer experiment that we performed in 4.2. and a more ventilated intermediate equatorial ocean. High values of mean kinetic energy are associated with higher oxygen values (Fig 9). This is particularly clear in GFDL01 at around 1500 m depth, where strong values of MKE are present and form the “bottom” of the low oxygen volume (oxygen lower than 50 mmol.m-3). Conversely GFDL025 and GFDL1 do not present high MKE values below 1000 m in the eastern part of the basin; the low oxygen volume extends till depths greater than 2000 m. It suggests that intermediate currents participate in the ventilation of the eastern tropical ocean and thus in limiting the vertical extension of the OMZ.

Oxygen levels do not increase linearly with the currents strength, i.e while currents strength increase in GFDL1, GFDL025 and GFDL01, oxygen levels are relatively similar in GFDL1 and GFDL025 (see Fig 5 and Fig 9). The relatively small net balance between large fluxes of respiration and oxygen supply (Duteil et al., 2014) may be responsible for this behavior. If the supply is slightly higher compared to the consumption by respiration, it will lead to an increase of oxygen concentration. If it is slightly lower, the oxygen levels will decrease. A small difference in supply (e.g slightly weaker currents) may therefore lead to a large difference in oxygen levels when integrated over decades. For this reason, the impact of the EICS is more visible below 1000 m as the respiration decreases following a power-law with depth (Martin et al., 1987) and is therefore easier to offset even by a moderate oxygen supply.

Resolving explicitly the EICS results in a similar oxygen distribution to what Getzlaff and Dietze (2013) (GD13) achieved with a simple EICS parameterization (Fig 9a): to compensate for the “missing” EICS in UVIC, a coarse resolution model, they enhanced anisotropically the lateral diffusivity in the equatorial region. The oxygen levels from UVIC GD13 are shown in blue contours on top of the UVIC oxygen distribution (black) in Fig 9. Implementing this approach tends to

14

514 homogenize oxygen levels zonally, with an increase of the mean levels by 30-50 mmol.m^{-3} in the
515 eastern basin and a decrease of oxygen concentrations in the western basin. While this approach
516 may be useful to better represent the oxygen mean state, it however does not take in account the
517 potential variability and future evolution of the EICS.
518
519 **5. Summary and conclusions**
520 Intermediate Depth Waters (IDW) are subducted in the Southern Ocean and transported
521 equatorward to the tropics by isopycnal processes (Sloyan and Kamenkovich, 2007; Sallee et al.,
522 2013; Meijers, 2014). At lower latitudes they recirculate into the lower thermocline of the tropical
523 regions at 500 - 1500 m and into the EICS (Zenk et al., 2005; Marin et al., 2010; Cravatte et al.,
524 2012; 2017; Ascani et al., 2015; Menesguen et al., 2019) (see schema Fig 1). We show here that
525 the representation of this ventilation pathway is important to take into account when assessing
526 tropical oxygen levels and the extent of the OMZ in coupled biogeochemical circulation or climate
527 models. Particularly, we highlight two critical, yet typical, biases that hamper the correct
528 representation of the tropical oxygen levels.
529
530 5.1 Subducted IDW properties and tropical oxygen
531 First, the current generation of climate models, such as the CMIP5 models, show large deficiencies
532 in simulating IDW. Along with an unrealistic representation of IDW volume and properties when the
533 waters enter the subtropics, the models also lack the observed prominent oxygen maximum
534 associated with IDW. Restoring oxygen levels to observed concentrations at 30°S/30°N and at
535 1500 m depth in a coarse resolution model, comparable to CMIP5 climate models in terms of
536 resolution and oxygen bias, shows a significant impact on the lower thermocline (500 – 1500 m)
537 oxygen levels: a positive anomaly of 60 mmol.m^{-3} at midlatitudes translates into an oxygen
538 increase by 10 mmol-m^{-3} in tropical regions after 50 years of integration.
539
540 The equatorward transport of the anomaly in the subtropics is mostly due to isopycnal subgrid
541 scale mixing processes as shown by the NEMO2 budget analysis. It suggests that mesoscale
542 activity plays a major role in transporting IDW equatorward. In addition subsurface eddies may
543 transport oxygen westward from the eastern Pacific ocean toward the mid-Pacific ocean region
544 (Frenger et al., 2018, see their Fig 2).
545
546 5.2 IMW transport and Equatorial Intermediate Current System
547 Second, the Equatorial Intermediate Current System (EICS) is not represented in coarse
548 resolution models and only poorly represented in high resolution ocean circulation models (0.25°
549 and 0.1°), as its strength remains too weak by a factor of two (consistent with previous studies, e.g
550 Ascani et al., 2015). The EICS transports the IDW that occupies the lower thermocline (500 – 1500

m depth) and the recirculation of the IDWin the tropical ocean, as suggested by the observational study of Zenk et al. (2005), and shown in our study.

We investigated the impact of the EICS on the oxygen supply with tracer release experiments: the concentration of a conservative tracer that originates from the subtropical ocean, is, after 50 years, 30 % higher in the eastern equatorial (5°N-5S) Pacific in an ocean model with 0.1° resolution, compared to an ocean model with 0.5 ° resolution. As the oxygen gradient along the equator is similar to the gradient of the conservative tracer, we assume a similar enhancement of oxygen supply by 30 % in the eastern equatorial Pacific at the same time scale. This means, if we account for oxygen consumption due to respiration (about 1 $mmol.m^{-3}.yr^{-1}$ between 5°N-5°S, see section 3.2), that the better resolved EICS in the higher resolution ocean leads roughly to higher intermediate oxygen levels of 15 - 30 $mmol\text{-}m^{-3}$ compared to the lower resolution ocean experiment in a timescale of 50 years. Consistently, the 0.1°-ocean GFDL01 model displays oxygen concentrations larger by about 30 $mmol.m^{-3}$ in the eastern equatorial lower thermocline (500-1500 m) compared to the 1°-ocean GFDL1 configuration (with higher subtropical oxygen concentrations of IWM of 15 $mmol.m^{-3}$ in GFDL01 at 30°S)

We would like to highlight two potential implications of our finding of the important role of the EICS for the Pacific eastern tropical oxygen supply: i) First, we have shown that the intermediate current system EICS is important for the connection between the western and eastern Pacific Ocean at a decadal / multidecadal time scale. This suggests that the EICS modulates the mean state and the variability of the tropical oxygen in the lower thermocline, and subsequently the whole water column by upwelling of deep waters. ii) Second, we have found an enhancement of the connections between the equatorial deep ocean (> 2000 m) and the lower thermocline if the resolution of a model is enhanced. This result is consistent with the studies of Brandt et al. (2011, 2012), who suggested, based on observational data and on an idealized model, that Equatorial Deep Jets as part of the EICS (see Fig 1b) propagate their energy upward and impact the upper ocean properties of the ocean, including their oxygen content. Taken this into account, we hypothesize that the Pacific Deep Water has a larger role than previously thought in modulating the intermediate and upper ocean properties.

A pragmatic approach to account for the missing EICS is to increase diffusion anisotropically, with increased zonal mixing in the tropics (Getzlaff and Dietze, 2013). This parameterization mimics a more vigorous EICS and improves the simulated shape of the OMZ in climate models. However, the prominent bias of IDW in climate models, and therefore of the water masses entering the EICS is not accounted for with this parameterization. Furthermore such a parameterization improves the mean state but does not reproduce the variability of the EICS.

16

588
589 5.3 Implication for biogeochemical cycles
590 The IDW are an important important supplier of oxygen to the tropical oceans, but also of nutrients
591 (Palter et al., 2010) as well as anthropogenic carbon (e.g Kathiwala et al., 2012), which
592 accumulates in mode and intermediate waters of the Southern Ocean (Sabine et al., 2004;
593 Resplandy et al., 2013). The mechanisms that we discussed here may therefore play a role in
594 ocean carbon climate feedbacks on time scales of decades to a century.
595
596 This study shows that there is a need to look with greater care into IDW properties to understand
597 the tropical oxygen distribution in models, in particular in CMIP class models. As shown by
598 Kwiatkowski et al. (2020), CMIP6 models (typical horizontal resolution of 1°) do not agree on the
599 future change in tropical oxygen levels (mean 100 – 600m, their Fig 2). This may partly originate in
600 a misrepresentation of the properties of the IDW in the different models and the strength of the
601 connection between western and eastern Pacific Ocean. Simple analyses, similar to our Fig 2
602 (oxygen levels at 30°S and oxygen levels in the eastern tropical Pacific) and Fig 9 (Mean Kinetic
603 Energy at intermediate depth) may give some insight into the mechanisms at play. In addition,
604 analyses of experiments performed in the context of the High Resolution Model Intercomparison
605 Project (resolution greater than 0.25°) (Haarsma et al., 2016), part of CMIP6, will give a more
606 complete insight on whether a significant Equatorial Intermediate Current System develops at
607 higher resolution. While HighResMIP are not coupled with a biogeochemical module, velocity fields
608 are available at a monthly resolution, which allows to perform “offline” tracer or Lagrangian particle
609 experiments.
610
611 Finally, this study suggests that changes of the properties of the IDW may contribute to the still
612 partly unexplained deoxygenation of 5 $mmol.m^{-3}$ / decade occurring in the lower thermocline of the
613 equatorial eastern Pacific Ocean (Schmidtko et al., 2017; Oschlies et al., 2018). In addition to an
614 oxygen decrease in tropical regions, Schmidtko et al. (2017) showed a decrease of oxygen levels
615 by 2-5 $mmol.m^{-3}$ in the regions of formations of AAIW. Based on repeated cruise observations,
616 Panassa et al. (2018) highlighted an increase of the apparent oxygen utilization in the core of the
617 AAIW, together with a 5 % increase in nutrient concentrations from 1990 to 2014. The transport of
618 this modified AAIW, poorer in oxygen and richer in nutrients, toward the low latitudes both by small
619 scale processes (section 3) and at the equator by the EICS (section 4), may explain a significant
620 part of the occurring deoxygenation in the equatorial ocean. In addition to changes in the AAIW
621 properties, little is known about the variability and long term trend of the strength of the EICS, an
622 oceanic “bridge” between the western and the eastern part of the basin. After our first steps toward
623 assessing the role of extratropical oxygen characteristics and the zonal transport of waters at
624 intermediate depths for tropical oxygen concentration, a possible way forward to further assess this

cascade of biases could be to perform idealized model experiments in high resolution configurations, aiming to assess both the effect of the observed change in the AAIW properties and of a potential change of EICS strength on oxygen levels.

Data and code availability

The code for the Nucleus for European Modeling of the Ocean (NEMO) is available at: https://www.nemo-ocean.eu/. The code for the University of Victoria (UVIC) model is available at :http://terra.seos.uvic.ca/model/. The Lagrangian particles ARIANE code is available at http://stockage.univ-brest.fr/~grima/Ariane/. The Coordinated Ocean-ice Reference Experiments (COREv2) dataset is available at: https://data1.gfdl.noaa.gov/nomads/forms/core/COREv2.html. The experiments data is available on request.

Authors contributions

OD conceived the study, performed the NEMO model and ARIANE experiments and analyzed the data. IF preprocessed and helped to analyze the GFDL data. JG preprocessed and helped to analyze the UVIC data. All authors discussed the results and wrote the manuscript.

Competing interest

The authors declare that they have no conflict of interest.

Acknowledgments

This work is a contribution of the SFB754 “Climate-Biogeochemistry Interactions in the Tropical Ocean”, supported by the Deutsche Forschungsgemeinschaft (DFG). The NEMO simulations were performed at the North German Supercomputing Alliance (HLRN). We would like to thank Markus Scheinert (research unit “Ocean Dynamics”, GEOMAR) for his technical support in compiling the NEMO code and for providing the high resolution NEMO input files. We would like to thank GFDL for producing the CM2-0 suite that involved a substantial commitment of computational resources and data storage. J.G acknowledges support by the project "Reduced Complexity Models" (supported by the Helmholtz Association of German Research Centres (HGF) – grant no. ZT-I-0010). I.F. acknowledges the German Federal Ministry of Education and Research (BMBF) project CUSCO (grant no. 03F0813A). O.D acknowledges the German Research Foundation (DFG) (grant no. 434479332)

References

18

659 Ascani, F., Firing, E., Dutrieux, P., McCreary, J. P., & Ishida, A. (2010). Deep Equatorial Ocean
660 Circulation Induced by a Forced–Dissipated Yanai Beam. Journal of Physical Oceanography,
661 40(5), 1118–1142. doi:10.1175/2010jpo4356.1
662 Ascani, F., Firing, E., McCreary, J. P., Brandt, P., & Greatbatch, R. J. (2015). The Deep Equatorial
663 Ocean Circulation in Wind-Forced Numerical Solutions. Journal of Physical Oceanography, 45(6),
664 1709–1734. doi:10.1175/jpo-d-14-0171.1
665 Bahl, A., Gnanadesikan, A., & Pradal, M. A. (2019). Variations in Ocean Deoxygenation Across
666 Earth System Models: Isolating the Role of Parameterized Lateral Mixing. Global Biogeochemical
667 Cycles, 33(6), 703–724. doi:10.1029/2018gb006121
668 Blanke, B., & Raynaud, S. (1997). Kinematics of the Pacific Equatorial Undercurrent: An Eulerian
669 and Lagrangian Approach from GCM Results. Journal of Physical Oceanography, 27(6), 1038–
670 1053. doi:10.1175/1520-0485(1997)027<1038:kotpeu>2.0.co;2
671 Brandt, P., Funk, A., Hormann, V., Dengler, M., Greatbatch, R. J., & Toole, J. M. (2011).
672 Interannual atmospheric variability forced by the deep equatorial Atlantic Ocean. Nature,
673 473(7348), 497–500. doi:10.1038/nature10013
674 Brandt, P., Greatbatch, R. J., Claus, M., DIDWischus, S.-H., Hormann, V., Funk, A., … Körtzinger,
675 A. (2012). Ventilation of the equatorial Atlantic by the equatorial deep jets. Journal of Geophysical
676 Research: Oceans, 117(C12), n/a–n/a. doi:10.1029/2012jc008118
677 Breitburg, D., Levin, L. A., Oschlies, A., Grégoire, M., Chavez, F. P., Conley, D. J., … Zhang, J.
678 (2018). Declining oxygen in the global ocean and coastal waters. Science, 359(6371), eaam7240.
679 doi:10.1126/science.aam7240
680 Busecke, J. J. M., Resplandy, L., & Dunne, J. P. (2019). The Equatorial Undercurrent and the
681 Oxygen Minimum Zone in the Pacific. Geophysical Research Letters, 46(12), 6716–6725.
682 doi:10.1029/2019gl082692
683 Cabré, A., Marinov, I., Bernardello, R., & Bianchi, D. (2015). Oxygen minimum zones in the tropical
684 Pacific across CMIP5 models: mean state differences and climate change trends. Biogeosciences,
685 12(18), 5429–5454. doi:10.5194/bg-12-5429-2015
686 Carrasco, C., Karstensen, J., & Farias, L. (2017). On the Nitrous Oxide Accumulation in
687 Intermediate Waters of the Eastern South Pacific Ocean. Frontiers in Marine Science, 4.
688 doi:10.3389/fmars.2017.00024
689 Cravatte, S., Kessler, W. S., & Marin, F. (2012). Intermediate Zonal Jets in the Tropical Pacific
690 Ocean Observed by Argo Floats. Journal of Physical Oceanography, 42(9), 1475–1485.
691 doi:10.1175/jpo-d-11-0206.1
692 Cravatte, S., Kestenare, E., Marin, F., Dutrieux, P., & Firing, E. (2017). Subthermocline and
693 Intermediate Zonal Currents in the Tropical Pacific Ocean: Paths and Vertical Structure. Journal of
694 Physical Oceanography, 47(9), 2305–2324. doi:10.1175/jpo-d-17-0043.1

Czeschel, R., Stramma, L., Schwarzkopf, F. U., Giese, B. S., Funk, A., and Karstensen, J. (2011), Middepth circulation of the eastern tropical South Pacific and its link to the oxygen minimum zone, J. Geophys. Res., 116, C01015, doi:10.1029/2010JC006565

Delworth, T. L., Rosati, A., Anderson, W., Adcroft, A. J., Balaji, V., Benson, R., … Zhang, R. (2012). Simulated Climate and Climate Change in the GFDL CM2.5 High-Resolution Coupled Climate Model. Journal of Climate, 25(8), 2755–2781. doi:10.1175/jcli-d-11-00316.1

Dietze, H., & Loeptien, U. (2013). Revisiting “nutrient trapping” in global coupled biogeochemical ocean circulation models. Global Biogeochemical Cycles, 27(2), 265–284. doi:10.1002/gbc.20029

Dufour, C. O., Griffies, S. M., de Souza, G. F., Frenger, I., Morrison, A. K., Palter, J. B., … Slater, R. D. (2015). Role of Mesoscale Eddies in Cross-Frontal Transport of Heat and Biogeochemical Tracers in the Southern Ocean. Journal of Physical Oceanography, 45(12), 3057–3081. doi:10.1175/jpo-d-14-0240.1

Duteil, O., & Oschlies, A. (2011). Sensitivity of simulated extent and future evolution of marine suboxia to mixing intensity. Geophysical Research Letters, 38(6), n/a–n/a. doi:10.1029/2011gl046877

Duteil, O., Koeve, W., Oschlies, A., Aumont, O., Bianchi, D., Bopp, L., … Segschneider, J. (2012). Preformed and regenerated phosphate in ocean general circulation models: can right total concentrations be wrong? Biogeosciences, 9(5), 1797–1807. doi:10.5194/bg-9-1797-2012

Duteil, O., Böning, C. W., & Oschlies, A. (2014). Variability in subtropical-tropical cells drives oxygen levels in the tropical Pacific Ocean. Geophysical Research Letters, 41(24), 8926–8934. doi:10.1002/2014gl061774

Duteil, O., Oschlies, A., & Böning, C. W. (2018). Pacific Decadal Oscillation and recent oxygen decline in the eastern tropical Pacific Ocean. Biogeosciences, 15(23), 7111–7126. doi:10.5194/bg-15-7111-2018

Duteil, O. (2019). Wind Synoptic Activity Increases Oxygen Levels in the Tropical Pacific Ocean. Geophysical Research Letters, 46(5), 2715–2725. doi:10.1029/2018gl081041

Eden, C., & Dengler, M. (2008). Stacked jets in the deep equatorial Atlantic Ocean. Journal of Geophysical Research, 113(C4). doi:10.1029/2007jc004298

Emery, W. J. 2003. Water types and water masses. In: Encyclopedia of Atmospheric Sciences. 2nd ed. (eds. J.R. Holton, J.A. Curry and J.A. Pyle). Elsevier, Atlanta, GA, pp. 1556–1567

Firing, E., Wijffels, S. E., & Hacker, P. (1998). Equatorial subthermocline currents across the Pacific. Journal of Geophysical Research: Oceans, 103(C10), 21413–21423. doi:10.1029/98jc01944

Firing, E. (1987). Deep zonal currents in the central equatorial Pacific. Journal of Marine Research, 45(4), 791–812. doi:10.1357/002224087788327163

Frenger, I., Bianchi, D., Stührenberg, C., Oschlies, A., Dunne, J., Deutsch, C., … Schütte, F. (2018). Biogeochemical Role of Subsurface Coherent Eddies in the Ocean: Tracer Cannonballs,

Hypoxic Storms, and Microbial Stewpots? Global Biogeochemical Cycles, 32(2), 226–249. doi:10.1002/2017gb005743

Galbraith, E. D., Dunne, J. P., Gnanadesikan, A., Slater, R. D., Sarmiento, J. L., Dufour, C. O., … Marvasti, S. S. (2015). Complex functionality with minimal computation: Promise and pitfalls of reduced-tracer ocean biogeochemistry models. Journal of Advances in Modeling Earth Systems, 7(4), 2012–2028. doi:10.1002/2015ms000463

Getzlaff, J., & Dietze, H. (2013). Effects of increased isopycnal diffusivity mimicking the unresolved equatorial intermediate current system in an earth system climate model. Geophysical Research Letters, 40(10), 2166–2170. doi:10.1002/grl.50419

Gnanadesikan, A., Bianchi, D., & Pradal, M. (2013). Critical role for mesoscale eddy diffusion in supplying oxygen to hypoxic ocean waters. Geophysical Research Letters, 40(19), 5194–5198. doi:10.1002/grl.50998

Gouriou, Y., Delcroix, T., & Eldin, G. (2006). Upper and intermediate circulation in the western equatorial Pacific Ocean in October 1999 and April 2000. Geophysical Research Letters, 33(10), n/a–n/a. doi:10.1029/2006gl025941

Griffies, S. M., Winton, M., Anderson, W. G., Benson, R., Delworth, T. L., Dufour, C. O., … Zhang, R. (2015). Impacts on Ocean Heat from Transient Mesoscale Eddies in a Hierarchy of Climate Models. Journal of Climate, 28(3), 952–977. doi:10.1175/jcli-d-14-00353.1

Haarsma, R. J., Roberts, M. J., Vidale, P. L., Senior, C. A., Bellucci, A., Bao, Q., Chang, P., Corti, S., Fučkar, N. S., Guemas, V., von Hardenberg, J., Hazeleger, W., Kodama, C., Koenigk, T., Leung, L. R., Lu, J., Luo, J.-J., Mao, J., Mizielinski, M. S., Mizuta, R., Nobre, P., Satoh, M., Scoccimarro, E., Semmler, T., Small, J., and von Storch, J.-S.(2016). High Resolution Model Intercomparison Project (HighResMIPv1.0)forCMIP6, Geosci. Model Dev., 9, 4185–4208, https://doi.org/10.5194/gmd-9-4185-2016

Iudicone, D., Rodgers, K. B., Schopp, R., & Madec, G. (2007). An Exchange Window for the Injection of Antarctic Intermediate Water into the South Pacific. Journal of Physical Oceanography, 37(1), 31–49. doi:10.1175/jpo2985.1

Izumo, T. (2005). The equatorial undercurrent, meridional overturning circulation, and their roles in mass and heat exchanges during El Niño events in the tropical Pacific ocean. Ocean Dynamics, 55(2), 110–123. doi:10.1007/s10236-005-0115-1

Khatiwala, S., Tanhua, T., Mikaloff Fletcher, S., Gerber, M., Doney, S. C., Graven, H. D., … Sabine, C. L. (2013). Global ocean storage of anthropogenic carbon. Biogeosciences, 10(4), 2169–2191. doi:10.5194/bg-10-2169-2013

Kawabe, M., & Fujio, S. (2010). Pacific ocean circulation based on observation. Journal of Oceanography, 66(3), 389–403. doi:10.1007/s10872-010-0034-8

Keller, D. P., Oschlies, A., & Eby, M. (2012). A new marine ecosystem model for the University of Victoria Earth System Climate Model. Geoscientific Model Development, 5(5), 1195–1220. doi:10.5194/gmd-5-1195-2012

Koshlyakov, M.N. and Tarakanov, R.Y. (2003). Antarctic Bottom Water in the Pacific sector of the Southern Ocean, Oceanology 43(1):1-15

Kriest, I., Khatiwala, S., & Oschlies, A. (2010). Towards an assessment of simple global marine biogeochemical models of different complexity. Progress in Oceanography, 86(3-4), 337–360. doi:10.1016/j.pocean.2010.05.002

Kwiatkowski, L., Torres, O., Bopp, L., Aumont, O., Chamberlain, M., Christian, J. R., Dunne, J. P., Gehlen, M., Ilyina, T., John, J. G., Lenton, A., Li, H., Lovenduski, N. S., Orr, J. C., Palmieri, J., Santana-Falcón, Y., Schwinger, J., Séférian, R., Stock, C. A., Tagliabue, A., Takano, Y., Tjiputra, J., Toyama, K., Tsujino, H., Watanabe, M., Yamamoto, A., Yool, A., and Ziehn, T.: Twenty-first century ocean warming, acidification, deoxygenation, and upper-ocean nutrient and primary production decline from CMIP6 model projections, Biogeosciences, 17, 3439–3470, https://doi.org/10.5194/bg-17-3439-2020, 2020.

Lachkar, Z., Orr, J. C., & Dutay, J.-C. (2009). Seasonal and mesoscale variability of oceanic transport of anthropogenic CO2. Biogeosciences, 6(11), 2509–2523. doi:10.5194/bg-6-2509-2009

Large, W. G., & Yeager, S. G. (2008). The global climatology of an interannually varying air–sea flux data set. Climate Dynamics, 33(2-3), 341–364. doi:10.1007/s00382-008-0441-3

Lübbecke, J. F., Böning, C. W., & Biastoch, A. (2008). Variability in the subtropical-tropical cells and its effect on near-surface temperature of the equatorial Pacific: a model study. Ocean Science, 4(1), 73–88. doi:10.5194/os-4-73-2008

Madec, G.., Bourdallé-Badie, R., Pierre-Antoine Bouttier, Bricaud, C., Bruciaferri, D., Calvert, D., Chanut, J., Clementi, E., Coward, A., Delrosso, D., Ethé, C., Flavoni, S., Graham, T., Harle, J., Iovino, D., Lea, D., Lévy, C., Lovato, T., Martin, N., … Vancoppenolle, M. (2017). NEMO ocean engine. https://doi.org/10.5281/ZENODO.3248739Marin, F., Kestenare, E., Delcroix, T., Durand, F., Cravatte, S., Eldin, G., & Bourdallé-Badie, R. (2010). Annual Reversal of the Equatorial Intermediate Current in the Pacific: Observations and Model Diagnostics. Journal of Physical Oceanography, 40(5), 915–933. doi:10.1175/2009jpo4318.1

Martin, J. H., Knauer, G. A., Karl, D. M., & Broenkow, W. W. (1987). VERTEX: carbon cycling in the northeast Pacific. Deep Sea Research Part A. Oceanographic Research Papers, 34(2), 267–285. doi:10.1016/0198-0149(87)90086-0

Meijers, A. J. S. (2014). The Southern Ocean in the Coupled Model Intercomparison Project phase 5. Philosophical Transactions of the Royal Society A: Mathematical, Physical and Engineering Sciences, 372(2019), 20130296. doi:10.1098/rsta.2013.0296

802 Ménesguen, C., Delpech, A., Marin, F., Cravatte, S., Schopp, R., & Morel, Y. (2019). Observations
803 and Mechanisms for the Formation of Deep Equatorial and Tropical Circulation. Earth and Space
804 Science, 6(3), 370–386. doi:10.1029/2018ea000438
805 Molinelli EJ (1981) The Antarctic influence on Antarctic Intermediate Water. J Mar Res 39:267–293
806 Oschlies, A., Brandt, P., Stramma, L., & Schmidtko, S. (2018). Drivers and mechanisms of ocean
807 deoxygenation. Nature Geoscience, 11(7), 467–473. doi:10.1038/s41561-018-0152-2
808 Palter, J. B., Sarmiento, J. L., Gnanadesikan, A., Simeon, J., and Slater, R. D. (2010). Fueling
809 export production: nutrient return pathways from the deep ocean and their dependence on the
810 Meridional Overturning Circulation, Biogeosciences, 7, 3549–3568, doi:10.5194/bg-7-3549-2010
811 Panassa, E., Santana-Casiano, J. M., González-Dávila, M., Hoppema, M., van Heuven, S. M. A. .,
812 Völker, C., … Hauck, J. (2018). Variability of nutrients and carbon dioxide in the Antarctic
813 Intermediate Water between 1990 and 2014. Ocean Dynamics, 68(3), 295–308.
814 doi:10.1007/s10236-018-1131-2
815 Pardo, P. C., Pérez, F. F., Velo, A., & Gilcoto, M. (2012). Water masses distribution in the
816 Southern Ocean: Improvement of an extended OMP (eOMP) analysis. Progress in Oceanography,
817 103, 92–105. doi:10.1016/j.pocean.2012.06.002
818 Paulmier, A., Ruiz-Pino (2009), D. Oxygen minimum zones (OMZs) in the modern ocean,Progress
819 in Oceanography, 80(3), 113-128, doi:10.1016/j.pocean.2008.08.001.
820 Qu, T., & Lindstrom, E. J. (2004). Northward Intrusion of Antarctic Intermediate Water in the
821 Western Pacific*. Journal of Physical Oceanography, 34(9), 2104–2118. doi:10.1175/1520-
822 0485(2004)034<2104:nioaiw>2.0.co;2
823 Resplandy, L., Bopp, L., Orr, J. C., & Dunne, J. P. (2013). Role of mode and intermediate waters in
824 future ocean acidification: Analysis of CMIP5 models. Geophysical Research Letters, 40(12),
825 3091–3095. doi:10.1002/grl.50414
826 Rowe, G. D., Firing, E., & Johnson, G. C. (2000). Pacific Equatorial Subsurface Countercurrent
827 Velocity, Transport, and Potential Vorticity*. Journal of Physical Oceanography, 30(6), 1172–1187.
828 doi:10.1175/1520-0485(2000)030<1172:pescvt>2.0.co;2
829 Russell, J. L., & Dickson, A. G. (2003). Variability in oxygen and nutrients in South Pacific Antarctic
830 Intermediate Water. Global Biogeochemical Cycles, 17(2), n/a–n/a. doi:10.1029/2000gb001317
831 Sabine, C. L. (2004). The Oceanic Sink for Anthropogenic CO2. Science, 305(5682), 367–371.
832 doi:10.1126/science.1097403
833 Sallée, J.-B., Shuckburgh, E., Bruneau, N., Meijers, A. J. S., Bracegirdle, T. J., Wang, Z., & Roy, T.
834 (2013). Assessment of Southern Ocean water mass circulation and characteristics in CMIP5
835 models: Historical bias and forcing response. Journal of Geophysical Research: Oceans, 118(4),
836 1830–1844. doi:10.1002/jgrc.20135
837 Schmidtko, S., Stramma, L., & Visbeck, M. (2017). Decline in global oceanic oxygen content during
838 the past five decades. Nature, 542(7641), 335–339. doi:10.1038/nature21399

Sen Gupta, A., & England, M. H. (2007). Evaluation of Interior Circulation in a High-Resolution Global Ocean Model. Part II: Southern Hemisphere Intermediate, Mode, and Thermocline Waters. Journal of Physical Oceanography, 37(11), 2612–2636. doi:10.1175/2007jpo3644.1

Shigemitsu, M., Yamamoto, A., Oka, A., & Yamanaka, Y. (2017). One possible uncertainty in CMIP5 projections of low-oxygen water volume in the Eastern Tropical Pacific. Global Biogeochemical Cycles, 31(5), 804–820. doi:10.1002/2016gb005447

Sloyan, B. M., & Kamenkovich, I. V. (2007). Simulation of Subantarctic Mode and Antarctic Intermediate Waters in Climate Models. Journal of Climate, 20(20), 5061–5080. doi:10.1175/jcli4295.1

Sloyan, B. M., & Rintoul, S. R. (2001). Circulation, Renewal, and Modification of Antarctic Mode and Intermediate Water*. Journal of Physical Oceanography, 31(4), 1005–1030. doi:10.1175/1520-0485(2001)031<1005:cramoa>2.0.co;2

Takano, Y., Ito, T., & Deutsch, C. (2018). Projected Centennial Oxygen Trends and Their Attribution to Distinct Ocean Climate Forcings. Global Biogeochemical Cycles, 32(9), 1329–1349. doi:10.1029/2018gb005939

Talley, L. D. (1993). Distribution and Formation of North Pacific Intermediate Water. Journal of Physical Oceanography, 23(3), 517–537. doi:10.1175/1520-0485(1993)023<0517:dafonp>2.0.co;2

Weaver, A. J., Eby, M., Wiebe, E. C., Bitz, C. M., Duffy, P. B., Ewen, T. L., … Yoshimori, M. (2001). The UVic earth system climate model: Model description, climatology, and applications to past, present and future climates. Atmosphere-Ocean, 39(4), 361–428. doi:10.1080/07055900.2001.9649686

Xu, L., Li, P., Xie, S. et al. (2016). Observing mesoscale eddy effects on mode-water subduction and transport in the North Pacific. Nature Communications, 10505 (2016), doi.org/10.1038/ncomms10505

Zenk, W., Siedler, G., Ishida, A., Holfort, J., Kashino, Y., Kuroda, Y., … Müller, T. J. (2005). Pathways and variability of the Antarctic Intermediate Water in the western equatorial Pacific Ocean. Progress in Oceanography, 67(1-2), 245–281. doi:10.1016/j.pocean.2005.05.003

Zhu, C., Liu, Z., & Gu, S. (2017). Model bias for South Atlantic Antarctic intermediate water in CMIP5. Climate Dynamics, 50(9-10), 3613–3624. doi:10.1007/s00382-017-3828-1

Figures and Table

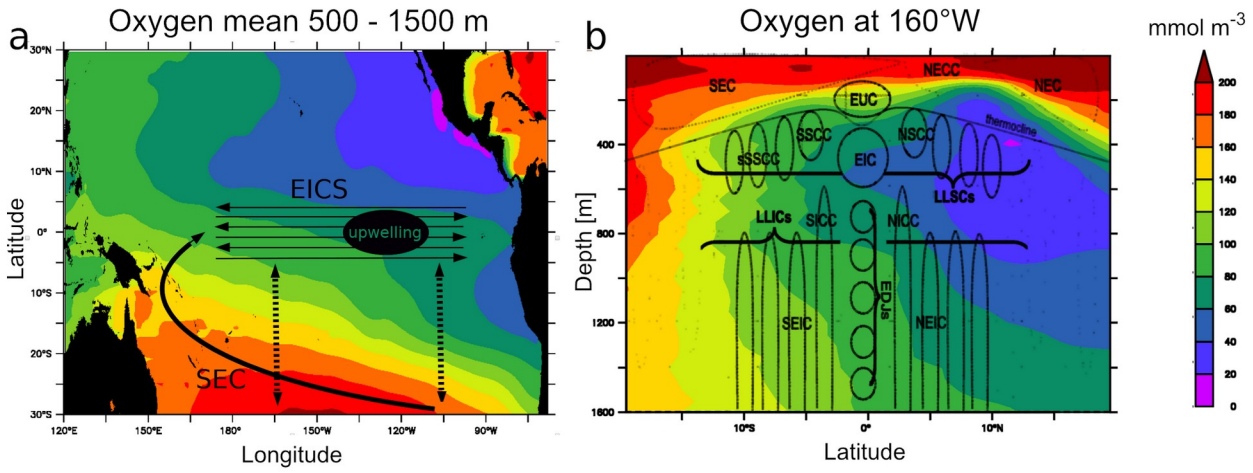

Figure 1 : a- schema summarizing the intermediate water masses (IWM) pathway from the subtropics into the equatorial regions. EICS : Equatorial Intermediate Current System. SEC : South Equatorial Current. Dashed line : isopycnal diffusive processes. Observed (World Ocean Atlas) oxygen levels (mmol.m^{-3}) in the lower thermocline (mean 500-1500m) are represented in color. b - schema (adapted from Menesguen et al., 2019) illustrating the complexity of the EICS, extending below the thermocline till more than 2000 m depth (see section 4.1 for a detailed description). Observed (World Ocean Atlas) oxygen levels at 160°W are represented in color. SEC : South Equatorial Current. N/SEC : North/South Equatorial Current. NECC: North Equatorial Counter Current. EUC : Equatorial Undercurrent. EIC : Equatorial Intermediate Current. N/SSCC : North /

25

South Subsurface Counter Current. LLSC : Low Latitude Subsurface Currents. LLIC : Low Latitudes Intermediate Currents. N/SEIC : North / South Equatorial Intermediate Current. N/SICC : North / South Intermediate Current. EDJ : Equatorial Deep Jets.

Figure 2 : a- oxygen levels (mmol.m^{-3}) in observations (World Ocean Atlas - WOA) (mean 500 – 1500 m) and models (UVIC, NEMO2, GFDL1, GFDL025, GFDL01). Contours correspond to WOA values. b: average “30°S” (120°E-65°W, 30°S) c : average “tropics” (160°W-coast, 20°N-20°S). d: average “30°S” vs “tropics”. e: average “30°S” vs volume of tropical suboxic ocean (oxygen lower than 20 mmol.m^{-3}) regions (1e15m3). b-e : UVIC : black, NEMO2 : cyan, GFDL1 : red, GFDL025, green; GFDL01 : blue, WOA: bold line (b,c) and star (d,e).

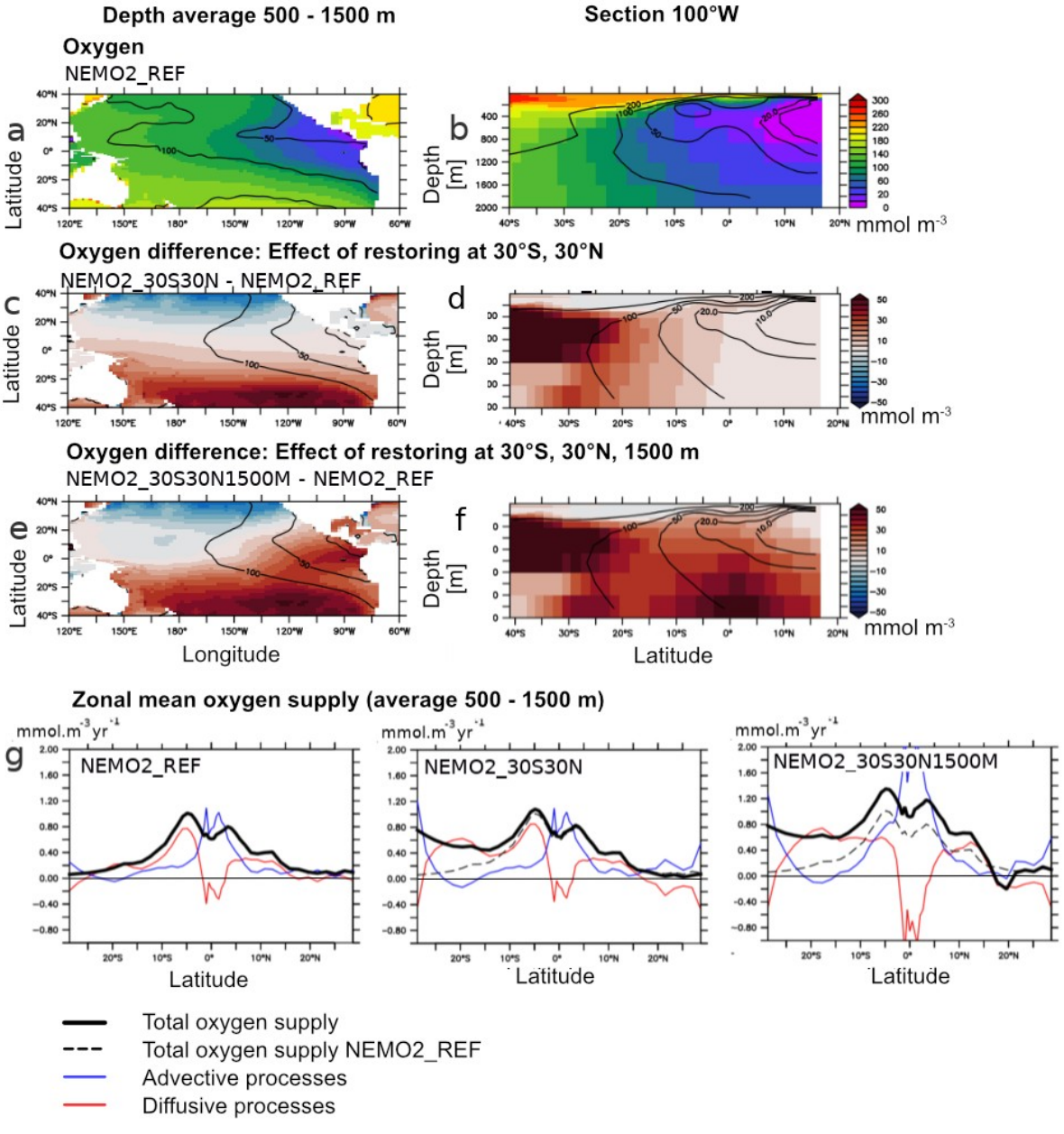

Figure 3 : a,b: Oxygen (mmol.m^{-3}) in the experiments NEMO2_REF (color) and World Ocean Atlas (contour) (a- average 500-1500 m, b- 100°W). c,d: Oxygen (mmol.m^{-3}) difference (c- average 500 – 1500m, d- 100°W) between the experiments NEMO2_30S30N minus NEMO2_REF. e,f : Oxygen (mmol.m^{-3}) difference (e- average 500-1500m, f- 100°W) between the experiments NEMO2_30S30N1500M minus NEMO2_REF. g- basin zonal average (average 500 - 1500 m) of the oxygen total supply (bold) (mmol.m^{-3}.year^{-1}), advective processes (blue) and isopycnal diffusion (red) in NEMO2_REF, NEMO2_30S30N, NEMO2_30S30N1500M. The dashed line is the oxygen total supply in NEMO2_REF.

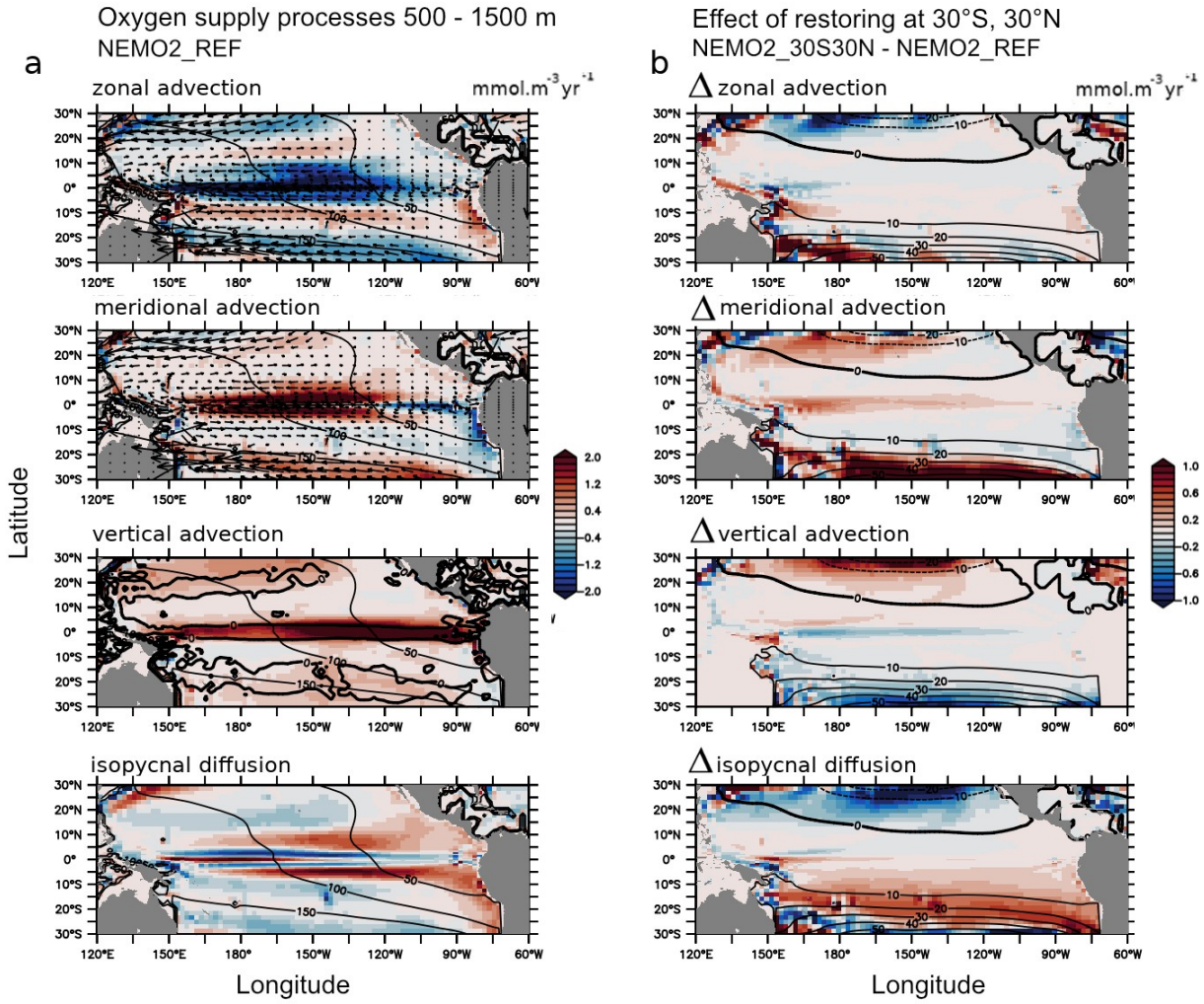

Figure 4 : a- Oxygen supply processes (mmol.m^{-3}.year^{-1} – average 500 - 1500m) in NEMO2_REF : zonal advection, meridional advection, vertical advection, isopycnal diffusion. The mean meridional and zonal currents are displayed as vectors (meridional, zonal advection). The mean vertical current (0 isoline) is represented as bold contour (vertical advection). Oxygen levels (mmol-m.$^{-3}$) are displayed in black contour. b- Difference in oxygen supply processes (mmol.m^{-3}.year^{-1} – average 500-1500m) between NEMO2_30S30N and NEMO2_REF : zonal advection, meridional

27

advection, vertical advection, isopycnal diffusion. The NEMO2_30S30N – NEMO2_REF oxygen anomaly (mmol.m^{-3}) is displayed in contour.

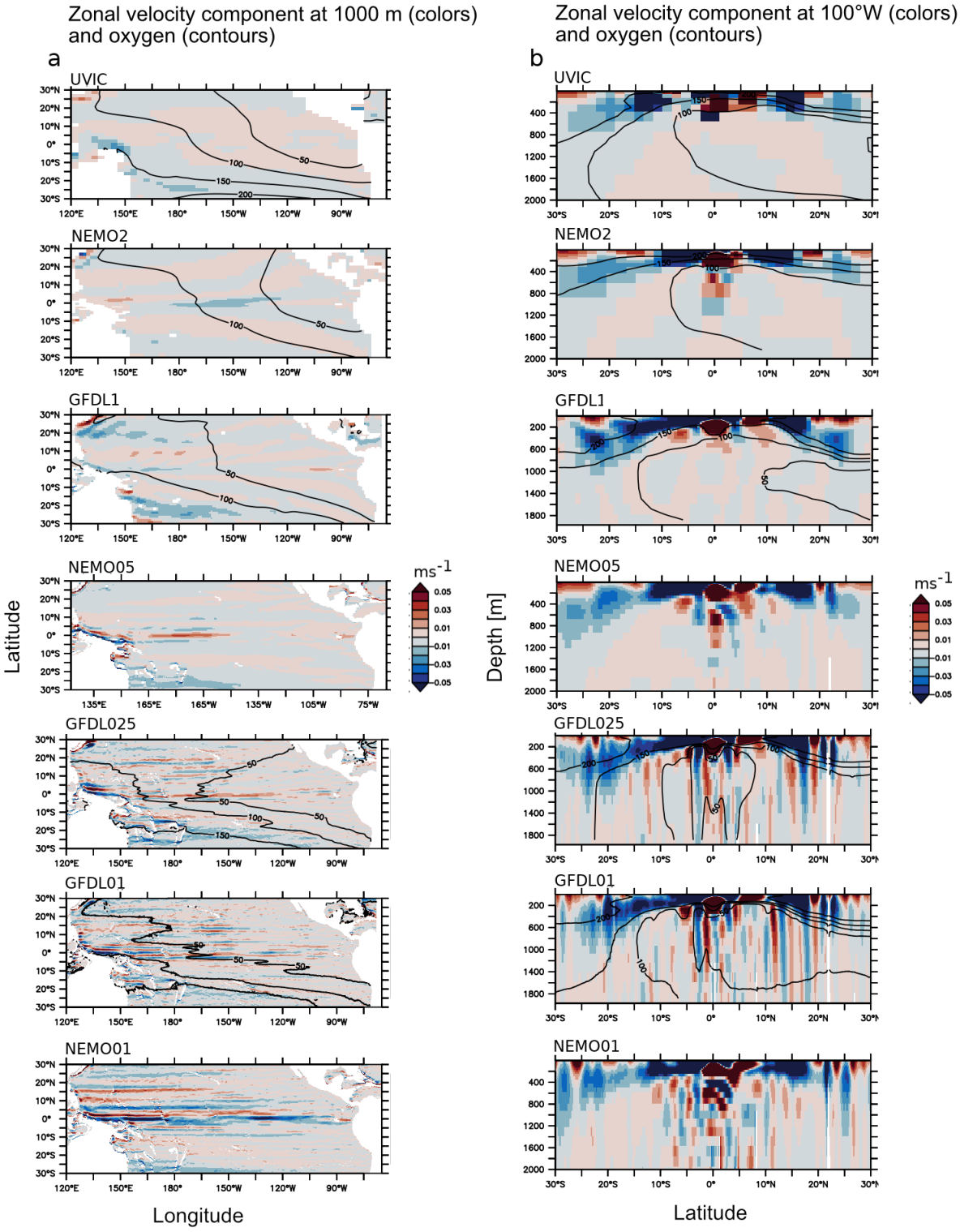

28

Figure 5 : mean currents velocity (ms^{-1}) at a- 1000 m depth b- 100°W in UVIC, NEMO2, NEMO05, GFDL025, GFDL01, NEMO01. The mean oxygen levels ($mmol.m^{-3}$) (when coupled circulation-biogeochemical experiments have been performed – see Table 1) are displayed in contour.

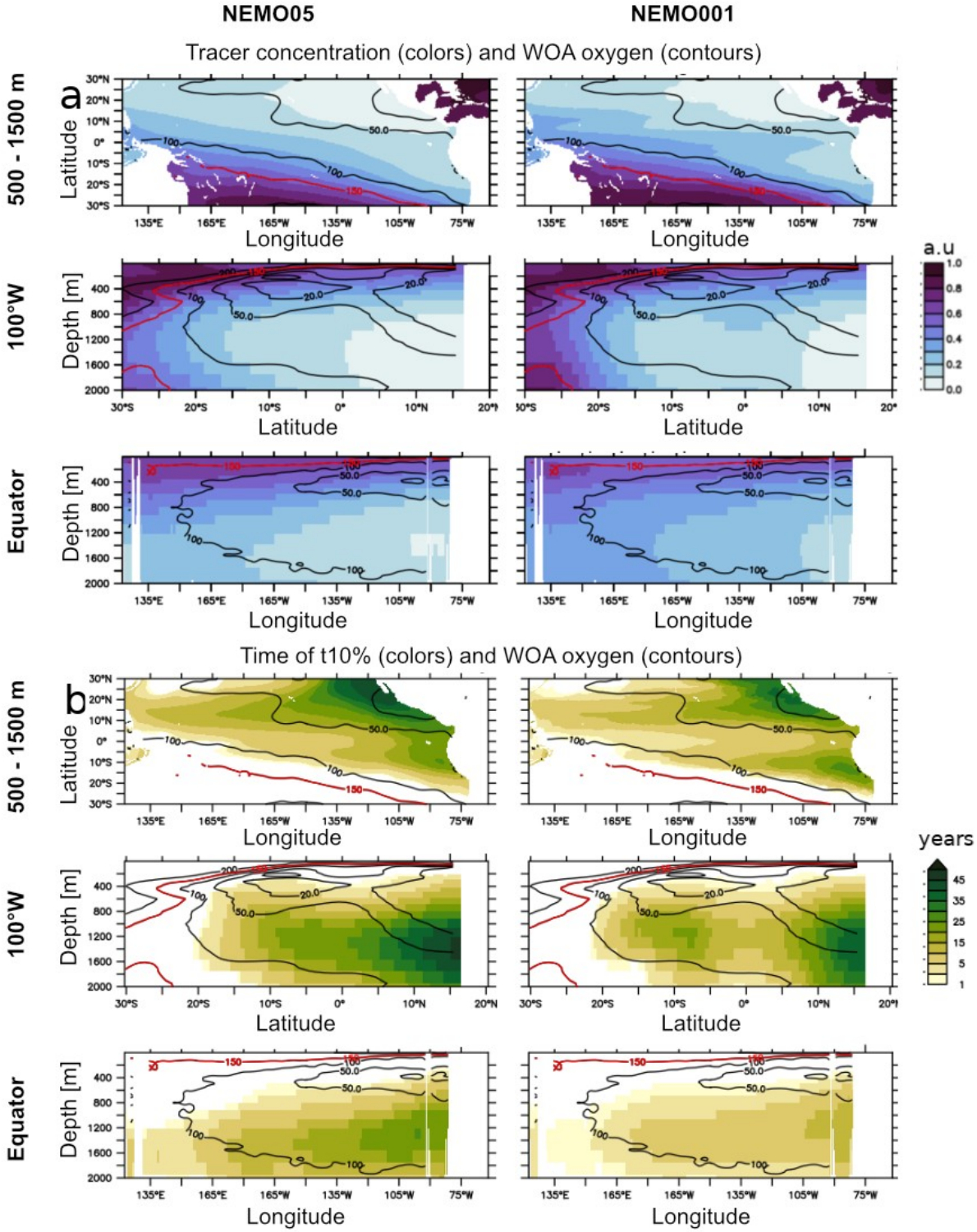

Figure 6: a : tracer concentration (arbitrary unit) after 60 years integration in NEMO05 and NEMO01: average 500-1500m, section 100°W, equatorial section. b: Time (years) at which the

29

released tracer reaches the concentration 0.1 (t10%) in NEMO05 and NEMO01: average 500-1500m, section 100°W, equatorial section. In all the subpanels, the WOA oxygen levels are displayed in contour. The red contour is the WOA 150 mmol.m^{-3} oxygen isoline, used to initialize the tracer level.

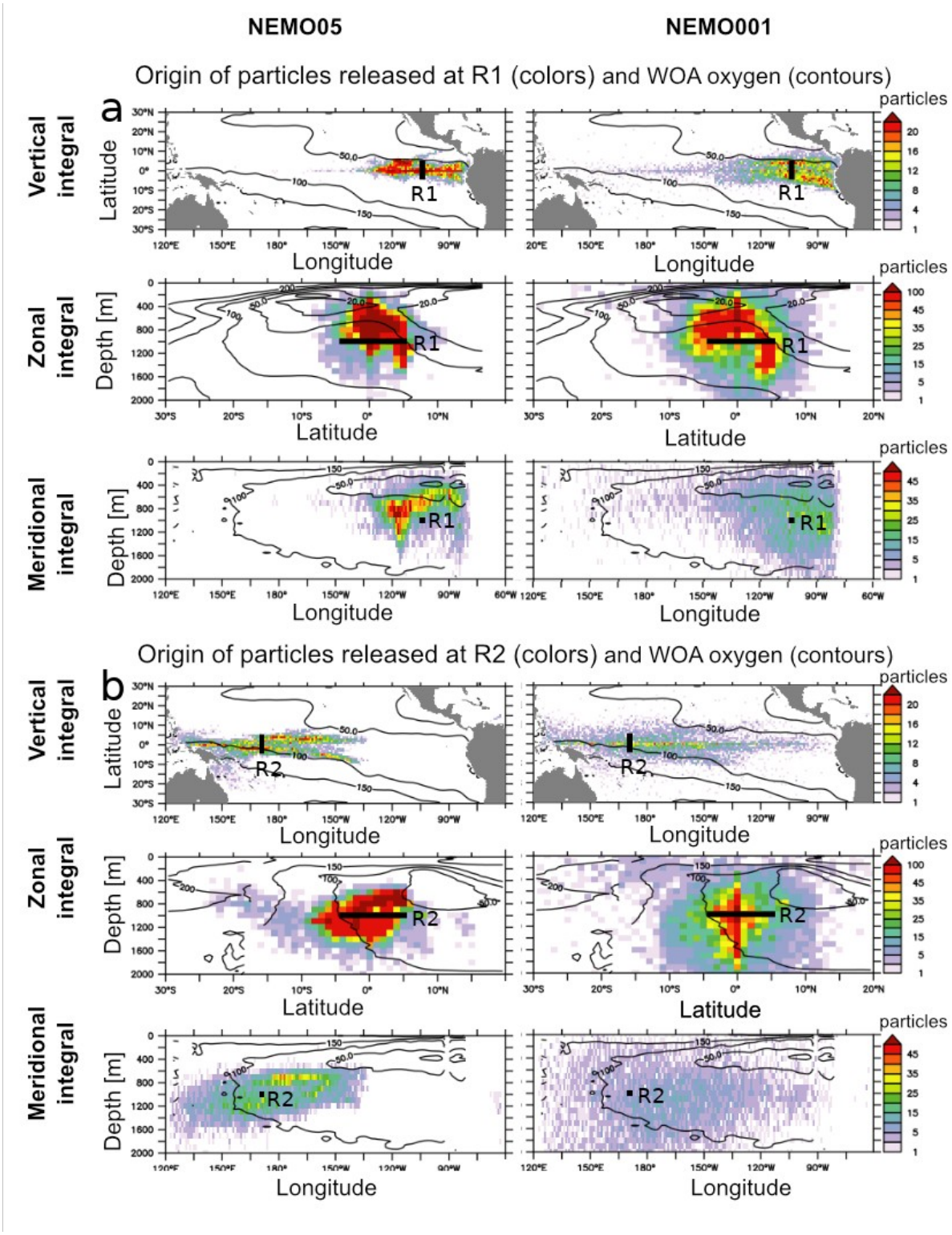

Figure 7 : Density (number of particles in a 1°x1°x100m depth box) distribution of the location of released Lagrangian particles (15 years backward integration starting from the final experiment

30

state) in NEMO05 and NEMO01. The release location is identified in bold and is located a- at 100°W/5°N-5S/1000 m depth (R1). b- at 160°E/5°N-5°S/1000 m depth (R2). The particles have been integrated vertically, zonally and meridionally. The observed mean oxygen levels (WOA) are displayed in contour.

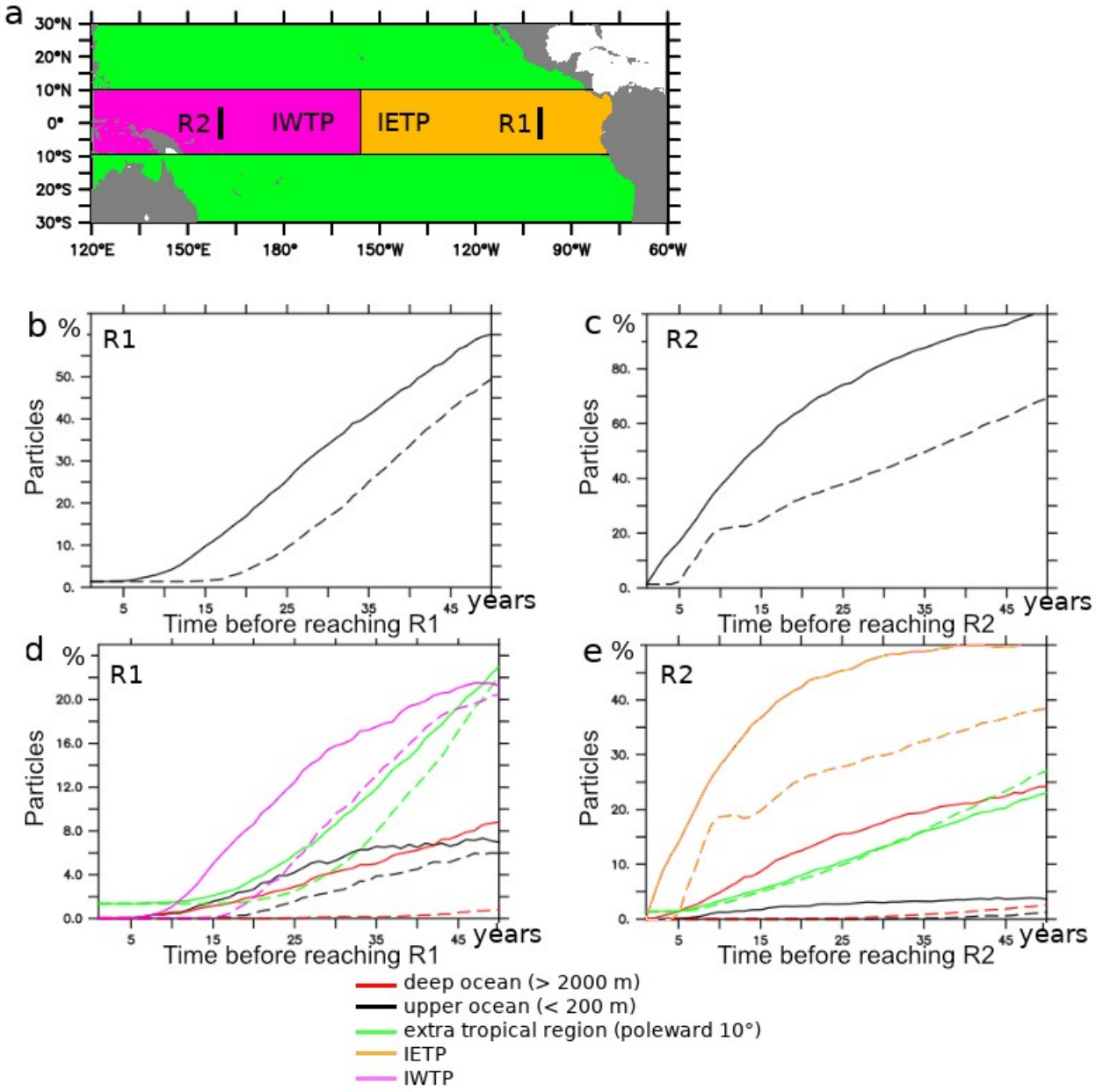

Figure 8 : a- schema summarizing the releases (R1: 100°W / 5°N-5°S / 1000 m , R2: 160°E / 5N°5S / 1000 m) location, the IETP (Intermediate Eastern Tropical Pacific), IWTP (Intermediate Western Tropical Pacific) regional extension. b. percentage of particles (release R1) originating from outside the IETP ocean region. b- percentage of particles (release R2) originating from outside the IWTP ocean region. d- percentage of particles (release R1) originating from the upper ocean (shallower than 200 m), the deeper ocean (deeper than 2000 m), subtropical regions

31

(poleward 10°), the IWTP. e- percentage of particles (release R2) originating from the upper ocean (shallower than 200 m), the deeper ocean (deeper than 2000 m), subtropical regions (poleward 10°), the IETP.

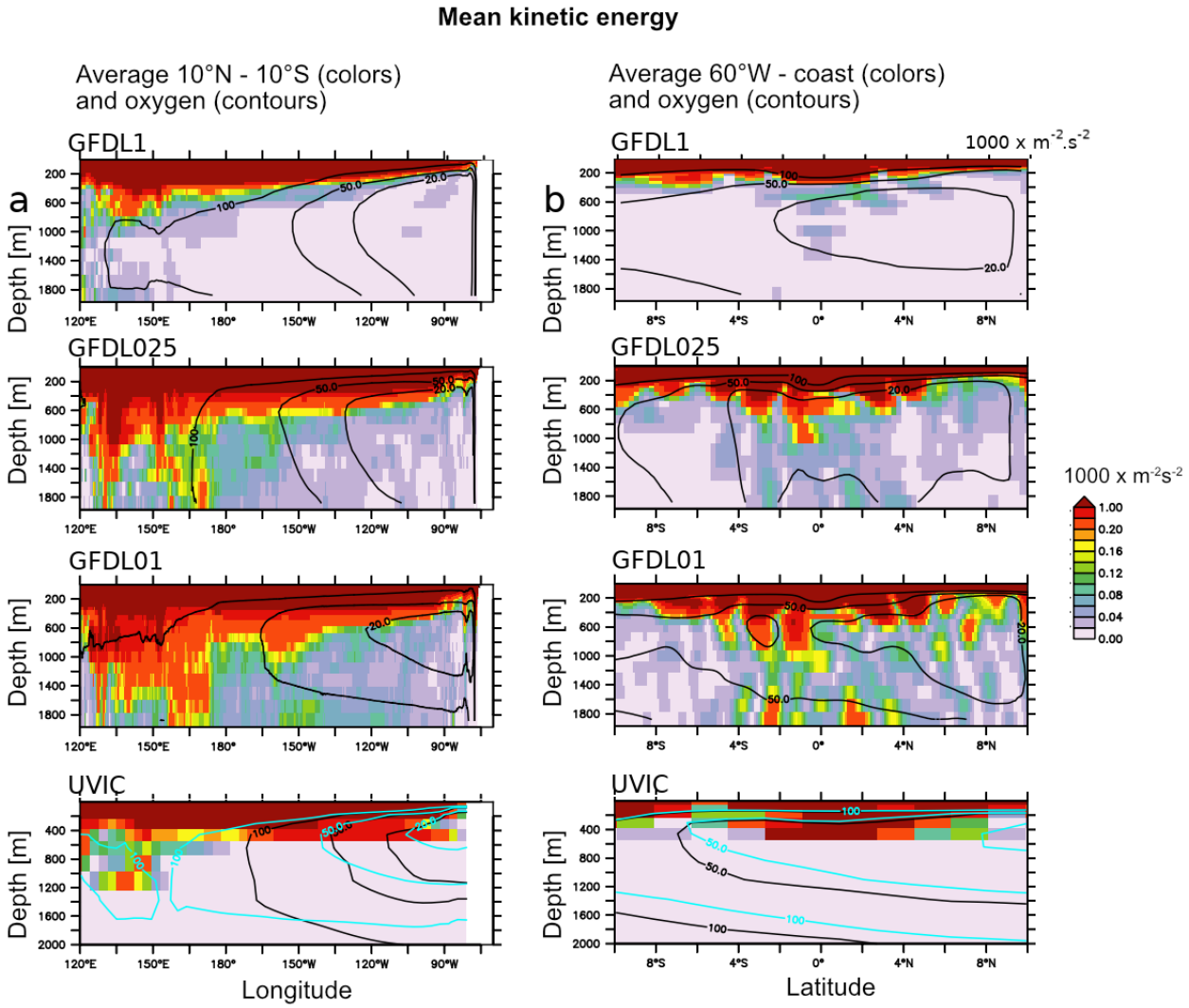

Figure 9 : a - Mean Kinetic Energy ($m2.s^{-2}$ x 1000) (average 10°N-10°S) in GFDL01, GFDL025, GFDL01, UVIC, b - similar to a. but average 160°W- coast. Oxygen levels ($mmol.m^{-3}$) are displayed in black contour. The blue contour corresponds to UVIC GD13 (Getzlaff and Dietze, 2013, including an anisotropical increase of lateral diffusion at the equator)

32

Table 1 :

Model	Resolution	Atmosphere	Integration (years)	BGC	Model Reference (circulation)	Model Reference (BGC)
Mean state comparison						
UVIC	2.8°	Coupled (temperature, humidity) Forced (NCEP/ NCAR wind stress)	10000	UVIC-BGC	Weaver et al., 2001	Keller et al., 2012
NEMO2	2° (0.5 eq)	Forced COREv2 "normal year"	1000	NPZD-O2	Madec et al., 2015	Kriest et al, 2010 Duteil et al., 2014
GFDL1	1°	Coupled	190	BLING	Delworth et al, 2012, Griffies et al, 2015	Galbraith et al., 2015
GFDL025	0.25 °	Coupled	190	BLING		
GFDL01	0.1°	Coupled	190	BLING		
Process oriented experiments						
Model	Resolution	Atmosphere	Integration (years)	BGC	Characteristics	
NEMO2 -REF -30N30S -30N30S1500M (section 2.2.1)	2° (0.5 eq)	Forced COREv2 1948-2007	60	NPZD-O2	- control experiment - O2 restoring to WOA at 30°N/30°S - O2 restoring to WOA at 30°N/30°S/1500m	
NEMO05 (section 2.2.2)	0.5°	Forced COREv2 1948 - 2007	60	Tracer release	- Tracer initialized to 1 (O2 WOA > 150 mmol.m-3) or 0 (O2 WOA < 150 mmol-m-3)	
NEMO01 (section 2.2.2)	0.1°	Forced COREv2 1948 – 2007	60	Tracer release		

33

Annex A

The differences in oxygen levels between the “models groups” (GFDL suite, UVIC, NEMO2) are partly related to differences in the atmospheric fields employed and the integration time (see 2).

1. Wind forcing

Zonal wind mean stress typically varies by 5 to 20 % between the different wind products (Chauduri et al., 2013). To test this impact, we performed an experiment using the UVIC model using 2 different wind products (NCEP and COREv2 – Large and Yeager, 2009) (Figure A1). While the shape of the OMZ shows slight differences, the volume of the OMZ and the mean oxygen levels in the tropical regions and in the mid latitudes are similar. Consistent with the Figure 2, higher oxygen levels at 30°S lead to higher oxygen levels in the tropical ocean and to a smaller OMZ volume (Figure A2)

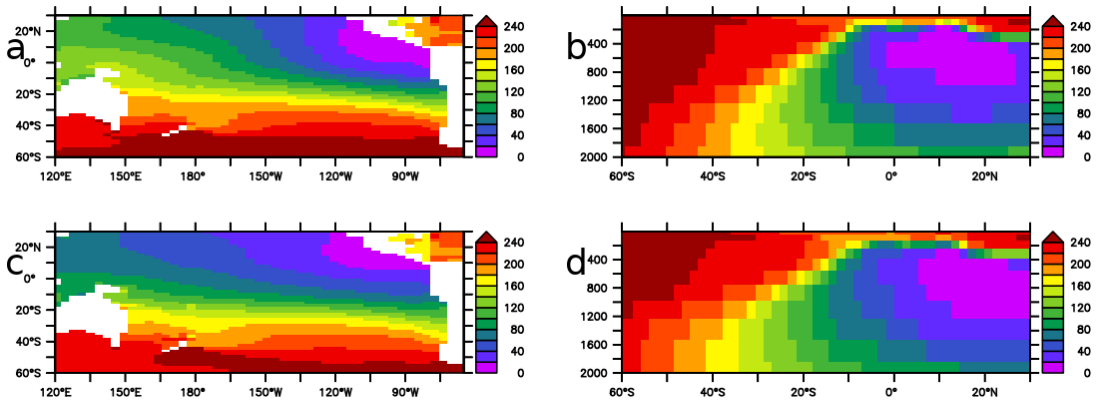

Figure A1 : Oxygen levels in UVIC (10000 years integration) a- mean 500-1500 m forcing NCEP. b- section 120°W forcing NCEP. c- mean 500-1500 m forcing COREv2, d- section 120°W forcing COREv2.

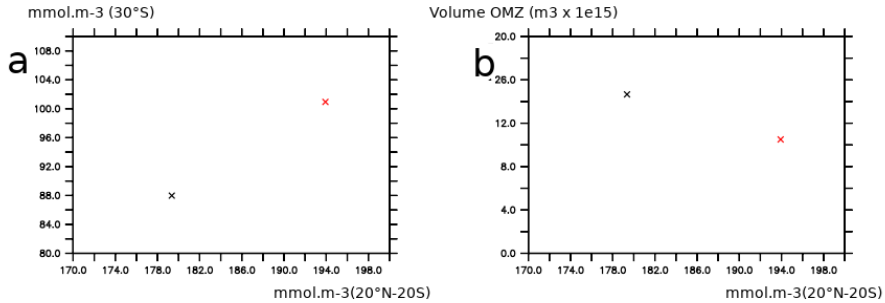

Figure A2 : a - Oxygen levels in UVIC (10000 years integration) at 30°S (zonal mean in the Pacific Ocean from surface to 2000 m depth) and in the tropical regions (20°S-20°N, averaged over the whole Pacific Ocean). b -

34

Oxygen levels in UVIC (10000 years integration) at 30°S (zonal mean in the Pacific Ocean, from surface to 2000 m depth) and volume of the OMZ in the Pacific Ocean. The configuration forced by COREv2 is shown in black, the configuration forced by NCEP is shown in red.

2. Spinup state

In complement, the spinup state of the model also impacts the oxygen levels as the deep ocean needs thousands of years to be in equilibrium. It may explain why UVIC (integrated for 10000 years) is characterized by much larger oxygen levels than the GFDL model suite (integrated for 190 years). As an example, the Figure A3 shows the evolution of oxygen levels during spinup in NEMO2. Larger oxygen levels at 30°S (e.g after 1000 years of integration) are characterized by a smaller OMZ volume (which is consistent with Fig 2) (Figure A4)

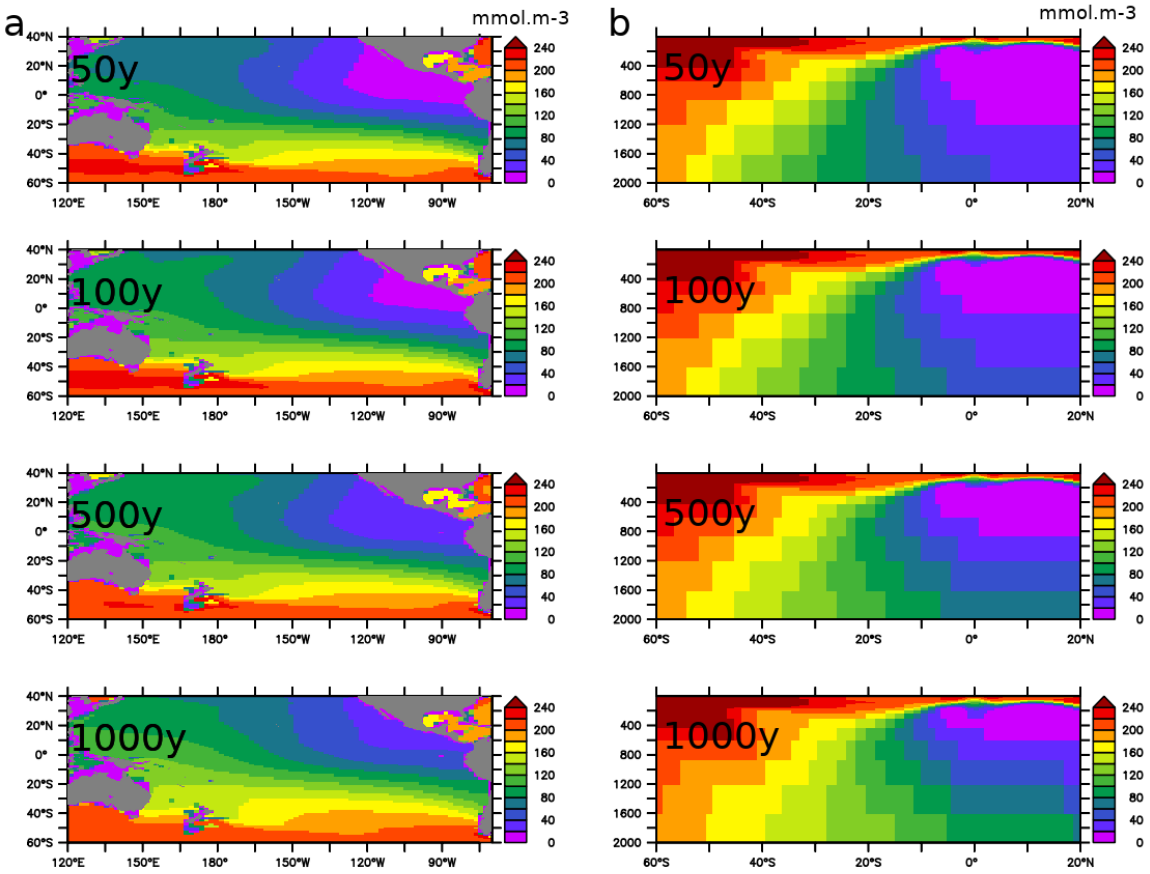

Figure A3 : oxygen levels at a - intermediate depth (average 500 – 2000 m) and b - 120°W in NEMO2 after 50, 100,500 and 1000 years integration

35

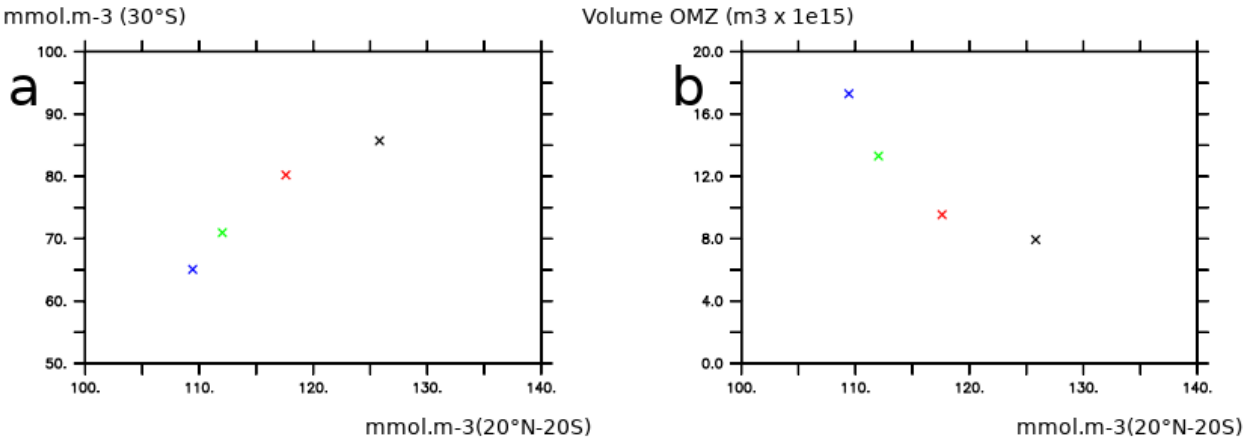

Figure A4 : a - Oxygen levels in NEMO2 at 30°S (zonal mean in the Pacific Ocean from surface to 2000 m depth) and in the tropical regions (20°S-20°N, averaged over the whole Pacific Ocean from surface to 2000 m depth). b - Oxygen levels in NEMO2 at 30°S (zonal mean in the Pacific Ocean from surface to 2000 m depth) and volume of the OMZ in the Pacific Ocean. The color of the cross depends of the integration duration (black : 50 years, red : 100 years, green : 500 years, blue 1000 years).

36

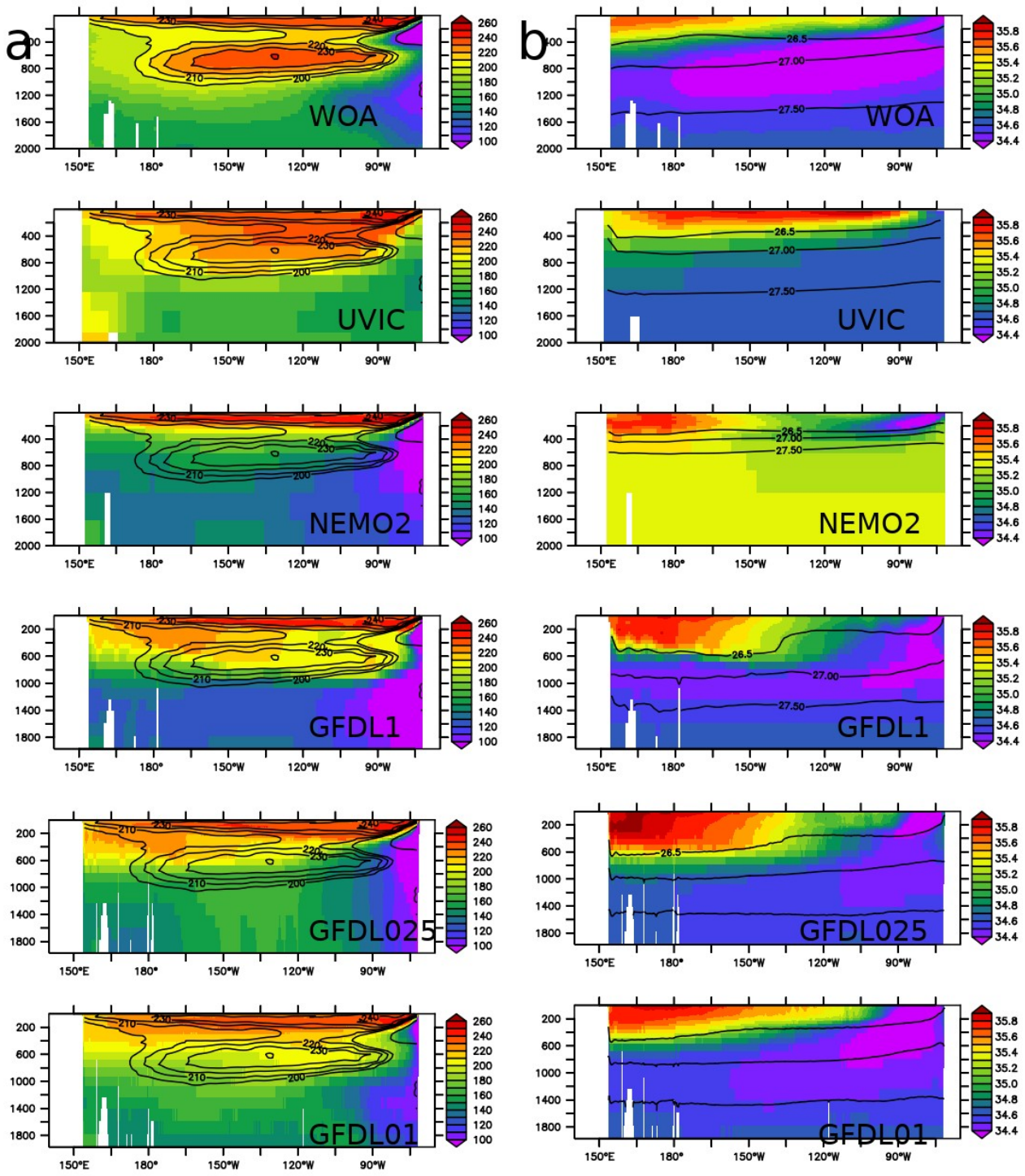

Figure A5 : a - oxygen levels (mmol.m-3) in observations and models at 30°S. The WOA oxygen levels are displayed in contour. b- salinity in observations and models at 30°S. The density anomaly (26.5, 27, 27.5) is displayed in contour.

37

1083 References

1084 Chaudhuri, Ayan & Ponte, Rui & Forget, Gael & Heimbach, Patrick. (2013). A Comparison of
1085 Atmospheric Reanalysis Surface Products over the Ocean and Implications for Uncertainties in Air-
1086 Sea Boundary Forcing. Journal of Climate. 26. 153-170. 10.1175/JCLI-D-12-00090.1.
1087 Large, W.G., Yeager, S.G. (2009). The global climatology of an interannually varying air–sea flux
1088 data set. Clim Dyn 33, 341–364. 10.1007/s00382-008-0441-3